VIBRATIONAL ENERGY TRANSFER

IN BROMINE MONOFLUORIDE

THESIS

Tim L. Thompson, Captain, USAF

AFIT/GEP/ENP/91D-8

REPORT DOCUMENTATION PAGE

Form Approved
OMB No. 0704-0188

1. AGENCY USE ONLY (Leave blank)	2. REPORT DATE	3. REPORT TYPE AND DATES COVERED
	DEC 91	MASTER'S THESIS

4. TITLE AND SUBTITLE
VIBRATIONAL ENERGY TRANSFER
IN BROMINE MONOFLUORIDE

5. FUNDING NUMBERS

6. AUTHOR(S)
TIMMIE L. THOMPSON, CAPT, USAF

7. PERFORMING ORGANIZATION NAME(S) AND ADDRESS(ES)
AIR FORCE INSTITUTE OF TECHNOLOGY
WPAFB, OH 45433-6583

8. PERFORMING ORGANIZATION REPORT NUMBER
AFIT/GEP/ENP/91D-8

10. SPONSORING/MONITORING AGENCY REPORT NUMBER
AFOSR/NE
Bolling AFB DC. 20332-6448

12a. DISTRIBUTION/AVAILABILITY STATEMENT
APPROVED FOR PUBLIC RELEASE;
DISTRIBUTION UNLIMITED.

12b. DISTRIBUTION CODE

13. ABSTRACT (Maximum 200 words)

Bromine monofluoride (BrF), an interhalogen molecule, is a prospective chemical laser candidate. This study continues research begun in characterizing radiative and collisional dynamics in BrF. Vibrational energy transfer in the $^3\Pi(0+)$ state of BrF is studied using time resolved laser induced fluorescence (LIF) techniques and observing the spectrally resolved emission.

First, vibrational transfer induced by the BrF production mix is determined to follow the Montroll-Shuler model and Landau-Teller scaling with a fundamental rate coefficient of $k_V(1,0) = (4.0 \pm 0.5) \times 10^{-12}$ cm^3/(molecules·seconds). Also, rate coefficients for the rare gases were found to scale with the reduced mass of the collision partner, as predicted by the Schwartz, Slawsky and Herzfeld (SSH) theory with values ranging from $(3.9 \pm 0.7) \times 10^{-12}$ cm^3/(molecules·seconds) for helium to $(2.2 \pm 0.3) \times 10^{-13}$ cm^3/(molecules·seconds) for xenon.

14. SUBJECT TERMS
Bromine monofluoride, interhalogens, vibrational energy transfer, laser induced fluorescence, rate coefficient, rare gases, Montroll-Shuler model

15. NUMBER OF PAGES
70

16. PRICE CODE

17. SECURITY CLASSIFICATION OF REPORT	18. SECURITY CLASSIFICATION OF THIS PAGE	19. SECURITY CLASSIFICATION OF ABSTRACT	20. LIMITATION OF ABSTRACT
UNCLASSIFIED	UNCLASSIFIED	UNCLASSIFIED	UL

AFIT/GEP/ENP/91D-8

VIBRATIONAL ENERGY TRANSFER IN BROMINE MONOFLUORIDE

THESIS

Presented to the Faculty of the School of Engineering
of the Air Force Institute of Technology
Air University
In Partial Fulfillment of the
Requirements for the Degree of
Master of Science in Engineering Physics

Tim L. Thompson, B.A., B.S.
Captain, USAF

December 1991

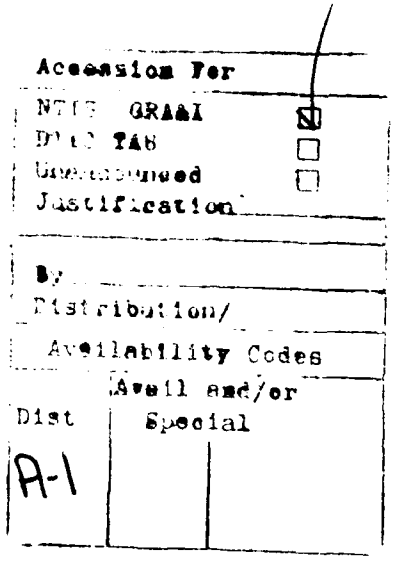

Approved for public release; distribution unlimited

Preface

This research has been but a small part of an overall effort at AFIT to characterize the diatomic interhalogens in determining potential candidates for visible chemical lasers. This thesis is a continuation of a study started by Capt David Melton in his doctorial research. The objective is to further characterize vibrational energy transfer in BrF(B) using pulsed, laser induced fluorescence techniques.

I owe thanks to many individuals for the successful completion of this research. My advisor, Capt Glen Perram, has given a lot of his time, effort, knowledge, and encouragement to me since I arrived at AFIT; to him I am very grateful. I am also indebted to Capt Melton for providing me a working apparatus and much of his experience in operating it. Thanks go to Mr. Rick Patton and Mr. Greg Smith for keeping all the equipment, and therefore the research, running smoothly. I want to also thank each of my classmates for their help and necessary social diversions needed to survive AFIT.

Lastly, I want to thank God and my wife Rina: For His design of the universe, which makes Physics the enjoyable challenge that it is, and for her love and support, which makes everything enjoyable.

– Tim Thompson

Table of Contents

List of Figures

List of Tables

Abstract

Bromine monofluoride (BrF), an interhalogen molecule, is a prospective chemical laser candidate. This study continues research begun in characterizing radiative and collisional dynamics in BrF. Vibrational energy transfer in the $^3\Pi(0+)$ state of BrF is studied using time resolved laser induced fluorescence (LIF) techniques and observing the spectrally resolved emission.

First, vibrational transfer induced by the BrF production mix is determined to follow the Montroll-Shuler model and Landau-Teller scaling with a fundamental rate coefficient of $k_v(1,0) = (4.0 \pm 0.5) \times 10^{-12}$ $cm^3/(molecules \cdot seconds)$. Also, rate coefficients for the rare gases were found to scale with the reduced mass of the collision partner, as predicted by the Schwartz, Slawsky and Herzfeld (SSH) theory with values ranging from $(3.9 \pm 0.7) \times 10^{-12}$ $cm^3/(molecules \cdot seconds)$ for helium to $(2.2 \pm 0.3) \times 10^{-13}$ $cm^3/(molecules \cdot seconds)$ for xenon.

VIBRATIONAL ENERGY TRANSFER IN BROMINE MONOFLUORIDE

I. Introduction

1.1 Motivation

The Department of Defense, specifically the Strategic Defense Initiative Organization (SDIO) and the Air Force, have recently shown great interest in visible chemical lasers. Chemical lasers are possibly well suited for space-based applications due to their relatively lightweight, self contained power supply. Visible chemical lasers have the additional benefit of short wavelength which reduces the size of the optics, reduces laser divergence and increases power on the target.[1] Other areas that can benefit from the research and development of the visible chemical laser are imaging and diagnostic missions, possible rocket fuels and high energy density materials.

The diatomic interhalogens look promising for possible chemical lasers.[2] The spectroscopy and kinetics of the interhalogens are reasonably well understood, the $B^3\Pi(0+) - X^1\Sigma^+$ transition in the interhalogens is in the visible region, and the B state can be excited by a variety of chemical pumping schemes. Iodine monofluoride and bromine monochloride have both been extensively studied for their potential as chemical lasers.[3,4]

A similar study of bromine monofluoride (BrF) as a potential chemical laser candidate is nearing completion. Lowe[5] and Melton[6] recently completed a study on the production of BrF, an unstable molecule, and on potential pumping schemes for creating excited BrF(B) molecules using $O_2(^1\Sigma)$. Melton also recently completed an investigation of electronic quenching of BrF(B) with a variety of collision partners.[6] The present research continues this detailed study of BrF by examining the rates of vibrational energy transfer for various vibrational levels and for various collision partners.

1.2 Problem Statement

Pulsed, laser induced fluorescence techniques will be used to investigate the vibrational energy transfer of BrF(B). Emissions from various vibrational levels of the B state of BrF will be spectrally resolved using a monochromator. The fluorescence intensity is directly proportional to the population of the vibrational state under observation. Therefore, observed fluorescence will indicate the distribution of population among the various vibrational states. As the excited BrF deactivates to lower vibrational levels the time profile will indicate the rate of the vibrational energy transfer.

Theoretical and computational models will be used to analyze the time profiles to determine the rate constants for vibrational transfer. A master rate equation and rate matrix is developed for this vibrational energy transfer. This coupled set of first order differential equations describe both electronic quenching and vibrational energy transfer. The

radiation and electronic quenching components of this matrix have been determined by Melton.[6] The Montroll-Shuler model, based on a set of harmonic oscillators and a number of simplifying assumptions, will be used in this analysis. The validity of these assumptions for the specific case of BrF will be evaluated.

The dependence of the rate coefficients on the BrF vibrational level, and on the characteristics of the buffer gas, including mass, will also be analyzed. The data will then be compared to previous data for BrF gathered by Clyne and Melton and compared to vibrational transfer rates for BrCl and IF found by Perram[3] and Wolf[4], respectively.

II. Background Theory

2.1 Chemical Laser Characteristics

Important characteristics a molecule must possess to be a potential candidate for a chemical laser were outlined by Davis.[2] First, it must have a moderately metastable excited state ($\tau_R \approx 10$ microseconds). A relatively long radiative lifetime is required to maintain a population inversion; however, extremely long lifetimes are not desirable because optical gain is directly proportional to the radiative rate. Collision-free lifetimes of some of the BrF B-state, v' levels are on the order of tens of microseconds (Table X, Appendix A), and meet this criteria. Collision-free losses are a result of radiation and predissociation only.

Predissociation is the radiationless transition from an excited molecule to separated atoms. It shortens the collision-free lifetime and depletes the B-state population through non-radiative processes. The interhalogens have a potential maximum within the B-state which provides stability for the lower vibrational levels (See Figure 1). In BrF, the onset of predissociation occurs at the v'= 7, J'= 29 level. Above this level BrF(B) is unstable.

A second characteristic required for a potential chemical laser molecule is low electronic quenching rates. This allows a relatively high density of reactants to be used without loss of energy from the B-

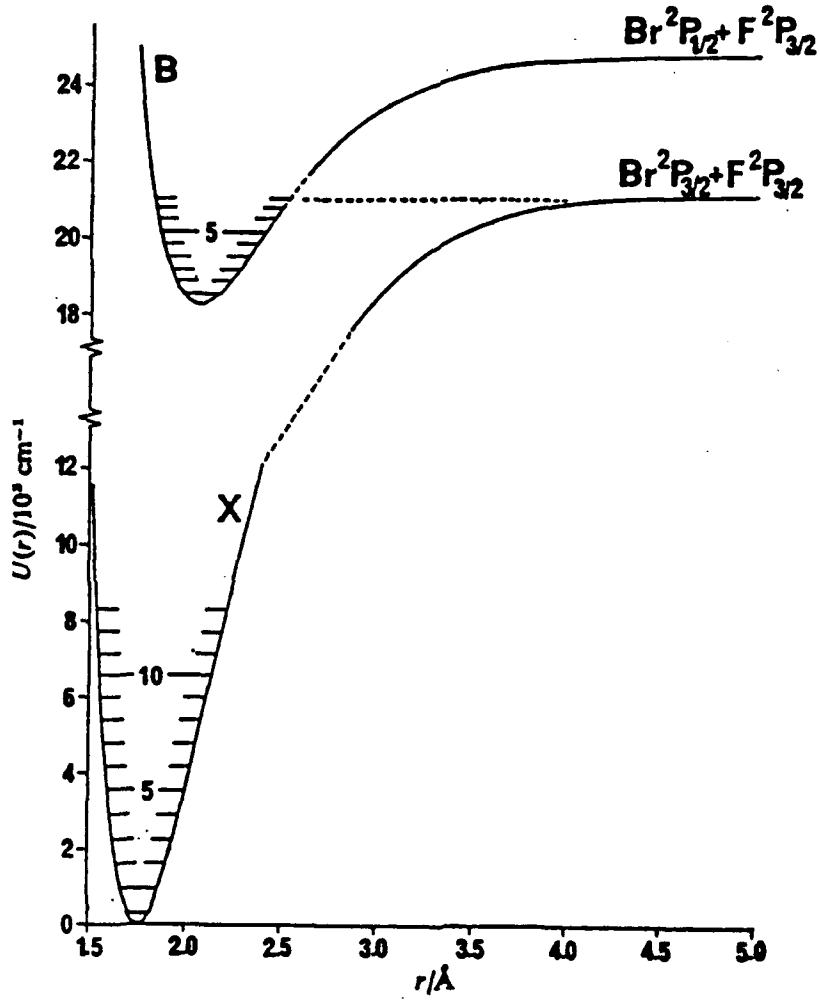

Figure 1. Potential Energy Curves for BrF^7

state through energy quenching collisions. Found in previous work,[6] BrF and other interhalogens have low self-quenching rates, on the order of $k_q = 3.4 \times 10^{-12}$ $cm^3/(molecule \cdot sec)$ for BrF, which allows a high reactant density.

A potential for a population inversion between the v' level in the B-state and the v" in the ground state is a third important characteristic for a potential chemical laser. As can be seen in Figure 1, the interhalogens, and BrF specifically, have a much higher equilibrium internuclear separation when in the B-state as compared to the ground state. Most probable radiative transitions from low vibrational levels (v'), as determined by Franck-Condon factors, will terminate on high vibrational levels (v") in the ground state. At relatively low temperatures (300 - 500°K) these vibrational levels will be vacant, most of the population will be thermalized in the v" = 0 state.

2.2 BrF and Interhalogen Spectroscopy

The halogen atoms, F, Cl, Br, I and At all have a ground state, outer shell electron configuration of s^2p^5. The diatomic interhalogens therefore have ground state, outer shell electronic configurations of $\sigma_g^2\pi_u^4\pi_g^4\sigma_u^0$, representing the symmetric $^1\Sigma^+$ state (see Figure 2), commonly called the X-state. Possible excited states for these molecules are created when an electron is excited to the empty σ level. One of these excited states is the $^3\Pi(0+)$ state, commonly called the B-

state. This study concentrates on vibrational energy transfer within this B-state.

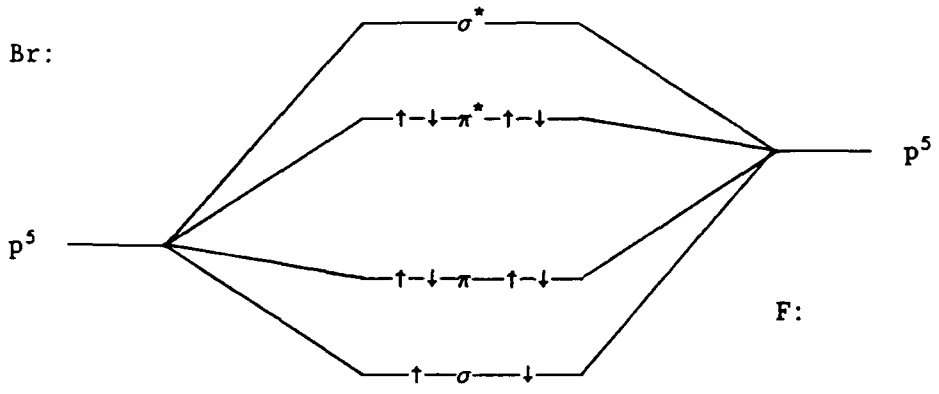

Figure 2. Relative Electronic Configuration of BrF(X)

A portion of the vibrationally-resolved spectrum of BrF, obtained by spectrally resolved laser induced fluorescence techniques, is shown in Figure 26 of Appendix A. The vibrational bands shown were determined by using the spectroscopic constants (Appendix A, Table XI) as determined by Coxon,[8] and calculated using the following equation[9]

$$h\nu = T_e - \omega_e(v+\frac{1}{2}) + \omega_e x_e(v+\frac{1}{2})^2 - \omega_e y_e(v+\frac{1}{2})^3 - \omega_e z_e(v+\frac{1}{2})^4 \quad (1)$$

where:

T_e is total electronic and vibrational energy for the excited state by vibrational level, v'.

w_e, $w_e x_e$, $w_e y_e$, and $w_e z_e$ are constants for the power series expansion of the vibrational levels due to anharmonicity of the potential curve.

and v is the vibrational quantum number in the ground state. As noted by Coxon, this is not a completely accurate representation of the vibrational levels in the B-state, but is adequate for making transition assignments for the moderate resolution of Figure 26.

As seen in Figure 26, not all transitions are equal in intensity. Different transitions have different intensities because of their Franck-Condon factors. For this work a computer code developed by the Phillips Laboratory was used to calculate the Franck-Condon factors from the RKR turning points found by Coxon. Table XII of Appendix A provides these Franck-Condon factors for ^{79}BrF.

2.3 Laser Induced Fluorescence (LIF)

LIF has revolutionized the science of spectroscopy by increasing the quality and quantity of data available and providing a direct method of studying the dynamics of excited states.[10] LIF uses a tunable dye laser to tune a high energy, narrow bandwidth, short pulse into coincidence with an absorption line of an atom or molecule. This directly excites a specific state of the atom or molecule and when these states relax they emit photons with energies equivalent to the spacing of the energy levels. By observing the time decay of this fluorescence, a determination of the collision-free or collisional kinetic processes involved can be made.

Using LIF in conjunction with a monochromator in the detection system, a detailed study of specific ro-vibrational states can be made. Without the monochromator or a system of narrow bandpass filters, observed radiation is the total fluorescence. This can be from any vibrational state or even unwanted fluorescence from impurities in the mix. With the addition of a monochromator, specific states can be pumped by the laser and specific, possibly different, states can be observed. Recording time profiles of the fluorescence provides a method of inferring the kinetics of the vibrational-translational energy transfer.

2.4 Kinetic Analysis

Melton[6] provides a good description of energy loss processes (shown in Figure 3) as occurring between rotational levels (3), between vibrational levels within an electronic state (2), between electronic states which can occur through quenching (4), or by emitting a photon (5), or loss of excitation energy by pre-dissociation to excited atoms (6). A change in energy level often involves a collision with a second body, M, which takes from the collision the difference in energy. This additional energy provided to the second body can either be translational, rotational, vibrational or even electronic, depending on the type of second body and its energy level spacings. For atomic species there will obviously be no rotational nor vibrational excitation.

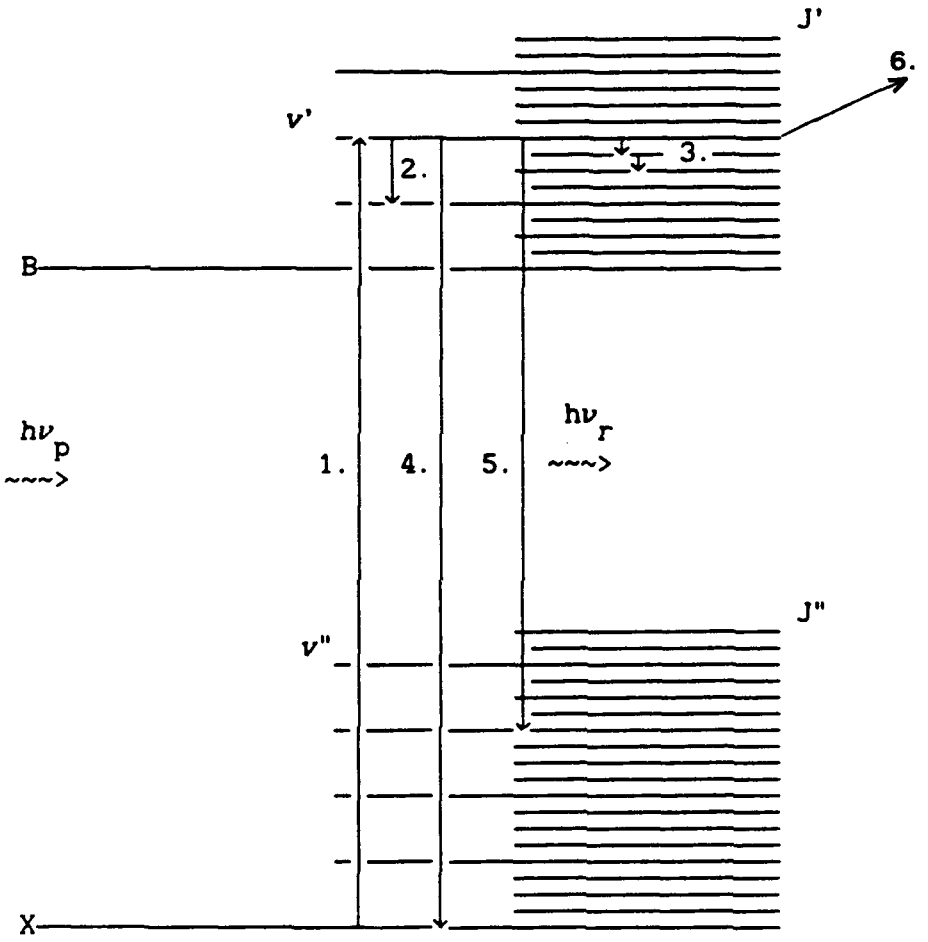

Figure 3. Energy Transfer Processes[6]

Assuming collisions of BrF involving atomic species, these energy transfer processes can be described by the following equations:

For rotational to translational collisions shown by transition 3 in Figure 3–

$$BrF(B;v',J') + M \xrightarrow{k_{R-T}} BrF(B;\ v',\ J' + \Delta J') + M \qquad (2)$$

For vibrational to translational collisions shown by transition 2 in Figure 3–

$$BrF(B;v',J') + M \xrightarrow{k_{V-T}} BrF(B;\ v' + \Delta v',\ J' + \Delta J) + M \qquad (3)$$

For electronic energy change when a photon is emitted as shown by transition 5–

$$BrF(B;v',J') \xrightarrow{1/\tau_r} BrF(X;\ v'',\ J'') + h\nu \qquad (4)$$

For electronic energy change by quenching, transition 4–

$$BrF(B;v',J') + M \xrightarrow{k_q} BrF + M \qquad (5)$$

For energy loss by pre-dissociation, shown by transition 6–

$$BrF(B;v',J') \xrightarrow{k_{pd}} Br^* + F^* \qquad (6)$$

If we concentrate on vibrational energy levels within a single electronic state and make some simplifying assumptions we can produce a master rate equation. Following a derivation by Perram,[11] we first assume that the collision partner is vibrationally inactive. Also, the excited species, BrF(B; v') is dilute enough so that no BrF(B; v') with

BrF(B; v') collisions take place, i.e. first order kinetics is assumed. Also assume that the quenching rate constant, k_q, is not a function of vibrational level. The third assumption is that the initial conditions create excited BrF(B; v') molecules in a specific vibrational level, v', below the pre-dissociation level. This is done by uniquely exciting BrF(X) with a laser tuned to a specific vibrational level. If N(v) is the number of molecules in a specific vibrational level, then

$$\frac{dN(v)}{dt} = \sum_{w} k(w \rightarrow v) N(w) M - N(v) \left[\frac{1}{\tau_r} + k_q M\right] - \sum_{w} k(v \rightarrow w) N(v) M \quad (7)$$

where k(w → v) is the rate constant for vibrational transfer from vibrational level w into v.

Let $Z(v,t) = \frac{N(v)}{N(v_o)} e^{t/\tau}$ be the time dependence of particles

in a specific vibrational state, and the initial condition (due to LIF) specifies that $N(v)|_{t=0} = N(v_o)|_{t=0}\delta_{v,vo}$. Substituting for N(v) and letting

$$\frac{1}{\tau} = \frac{1}{\tau_R} + k_q M \quad (8)$$

equation 7 can be simplified.

$$\frac{dN(v)}{dt} = N(v_o)\frac{dZ(v)}{dt}e^{-\frac{t}{\tau}} - N(v_o)\frac{Z(v)}{\tau}e^{-\frac{t}{\tau}}$$
$$- \sum_w k(w \rightarrow v) N(w_o) Z(w) e^{-\frac{t}{\tau}} M - N(v_o)\frac{Z(v)}{\tau}e^{-\frac{t}{\tau}} \qquad (9)$$
$$- \sum_w k(v \rightarrow w) N(v_o) Z(v) e^{-\frac{t}{\tau}} M$$

Canceling the second term and the exponential term from both sides of equation 9 and solving for $\frac{dZ(v)}{dt}$ yields

$$\frac{dZ(v)}{dt} = -\sum_w k(w \rightarrow v) Z(w) M - \sum_w k(v \rightarrow w) Z(v) M$$
$$- \sum_w k'(w \rightarrow v) Z(w) - k''(v) Z(v) \qquad (10)$$

where $k'(w \rightarrow v) = \sum_w k(w \rightarrow v) M$ and $k''(v) = \sum_w k(v \rightarrow w) M$. In matrix notation, this can be represented by $\frac{d\vec{Z}}{dt} = \vec{R}\vec{Z}$, where $\vec{R} = R_{vw} = k'(w \rightarrow v) - k''(v)\delta_{wv}$ is the rate matrix. If $\vec{R}$ is known, then equation 10 can be solved using eigenvector methods.

2.4.1 Landau-Teller Model. A theory developed by Landau and Teller[12] using first order perturbation theory is useful to describe vibrational relaxation. It assumes small transition-inducing perturbations in the internuclear separation distance for harmonic oscillators. Landau and Teller showed that the transition probability,

and therefore the rate constant, for any other level is simply a multiple of the vibrational quantum number, v, i.e. $k(v \rightarrow v-1) = vk(1 \rightarrow 0)$.

2.4.2 Detailed Balance. The principle of detailed balance states that the rate of transfer into an energy level must be equal to the rate of transfer out of that energy level at equilibrium. Also, at equilibrium the number of molecules at a higher energy level is a Boltzmann factor less than the number at a lower level, i.e.

$$N(v) = N(w)\, e^{\frac{-\Delta E}{k_B T}} \tag{11}$$

where $\Delta E = E_v - E_w$, is the difference in vibrational energy. Therefore, the upward rate constants $k(w \rightarrow v)$, where $w < v$, is a Boltzmann factor slower than the downward rate constant. This can be understood by recognizing that transitioning upward requires energy and transitioning downward releases energy.

Combining this with the results of the Landau-Teller model provides a convenient way to describe an upward transition from only the fundamental $1 \rightarrow 0$ rate coefficient.

$$k(v-1 \rightarrow v) = vk_v(1 \rightarrow 0)\, e^{\frac{-\Delta E}{k_B T}} \tag{12}$$

where $\Delta E = E_v - E_{v-1}$, is the difference in vibrational energy of the $v = 1$ and $v = 0$ vibrational level. Assuming no multiquantum transitions occur and using detailed balance and the Landau-Teller model, the rate

matrix is greatly simplified. In this case all rate coefficients are simply related to the fundamental rate coefficient, $k_v(1,0)$.

2.4.3 Montroll-Shuler Model. A solution to the rate equation using the Landau-Teller theory and assuming harmonic oscillators was found by Montroll and Shuler[13] in 1957. Their assumptions include low concentration of the excited state molecules immersed in a heat bath of inert molecules; radiative lifetimes and quenching rates independent of vibrational state; and vibrational transitions of $\Delta v = \pm 1$ only. Their solution to the rate equation for the population in a vibrational state n, for a disturbance that initially populates a single vibrational state m, is

$$Z_n(t) = \left[\frac{(1-e^{\theta})\,e^{m\theta}}{(e^{-\tau}-e^{\theta})}\right]\left[\frac{e^{-\tau}-1}{(e^{-\tau}-e^{\theta})}\right]^{m+n} F(-n,-m,1;U^2) \qquad (13)$$

where

$$\theta = h\nu/k_B T$$

$$U = \sinh(\theta/2)/\sinh(\tau/2)$$

$$\tau = k_v(1,0)(1 - e^{-\theta})t$$

F = Hypergeometric function

Equation 13 shows that vibrational transfer is determined from one rate coefficient, $k_v(1,0)$, and from this we can determine all the other rate constants from the Landau-Teller theory.

The validity of the Montroll-Shuler model is questionable for the case of BrF. The anharmonicity of BrF(B) is low, $w_e x_e/w_e = 0.009$. This

is higher than for the molecule IF ($w_e x_e/w_e$ = 0.007),[4] for which the Montroll-Shuler model has been shown valid, but lower than the anharmonicity of BrCl (0.013),[3] for which the model is not as valid. Also, the Montroll-Shuler model assumes vibrational transitions of $\Delta v = \pm 1$. For IF, the vibrational level spacing, compared to translational energy at room temperature, $\Delta E_v = h\nu/k_B T = 2.0$, is large, therefore multi-quantum transitions are unlikely. For BrCl, the spacing is approximately 1, and multi-quantum transitions are experimentally established at 40% of the $\Delta v = -1$ rate.[3] For BrF(B), where the vibrational spacing is 1.7, the situation is not as definite. Finally, the assumption of quenching and radiative lifetimes independent of vibrational level is valid for BrF(B) with $v' < 6$. Above this level, predissociation shortens the radiative lifetimes.

In this study a computer code developed by Melton[14] was used to fit equation 13 to the observed data. This code determined the fundamental $k_v(1,0)$ rate coefficient that produced the best fit to the data (see Figures 7 - 13). The code is written in PASCAL and runs on a Zenith-248 microcomputer. The model varies an initial guess of $k_v(1,0)$ through a simple stepping routine to minimize a least-squares merit function.

2.3.4 The Schwartz, Slawsky, and Herzfeld (SSH) Theory. The Landau-Teller theory was derived by neglecting the attractive part of the intermolecular potential. The SSH theory[15] includes an attractive part which increases the vibrational to translational transfer

probability by increasing the relative velocity. The result gives the same dependence on vibrational frequency, mass and temperature as the Landau-Teller theory, but includes an exponential term with the attractive part of the potential. If the vibrational spacing is relatively large, this exponential term will dominate and the logarithm of the transfer probability will be proportional to the (reduced mass)$^{\frac{1}{2}}$. The transfer probability, P, can be defined as

$$P = \frac{k_v}{k_g} = \frac{k_v}{\sigma g} \tag{14}$$

where $k_g = \sigma g$ is the gas kinetic or hard sphere rate coefficient,

$\sigma = \pi(r_1 + r_2)^2$ is the collision cross-section

$g = \left[\frac{8k_bT}{\pi\mu}\right]^{\frac{1}{2}}$ is the relative velocity

μ is the reduced mass of the colliding pair.

III. Description of Experiment

The apparatus used in this kinetic experiment of BrF is diagrammed in Figure 4. The experiment is naturally subdivided into the three parts discussed below: the flow system, the excitation system and the detection system. Before the raw data gathered from the fluorescence measurements can be interpreted it has to undergo a series of data reduction steps. This will also be described.

3.1 Flow System and Chamber

Since BrF is a kinetically unstable molecule, a flow system is used that provides a continuous supply of newly created BrF. The BrF is produced immediately prior to entering the fluorescence cell by the reaction:

$$F + Br_2 \rightarrow BrF + Br \qquad (15)$$

Bemand and Clyne[16] reported that this reaction has a rate coefficient at 298°K of $(2.2\pm1.1)\ x10^{-10}\ cm^3/sec$. An excess of F atoms is used to avoid leaving any nonreacting Br_2 molecules that have a strong Br_2 fluorescence for excitation wavelengths longer than approximately 5200Å. At wavelengths shorter than this Br_2 is photo-dissociated.

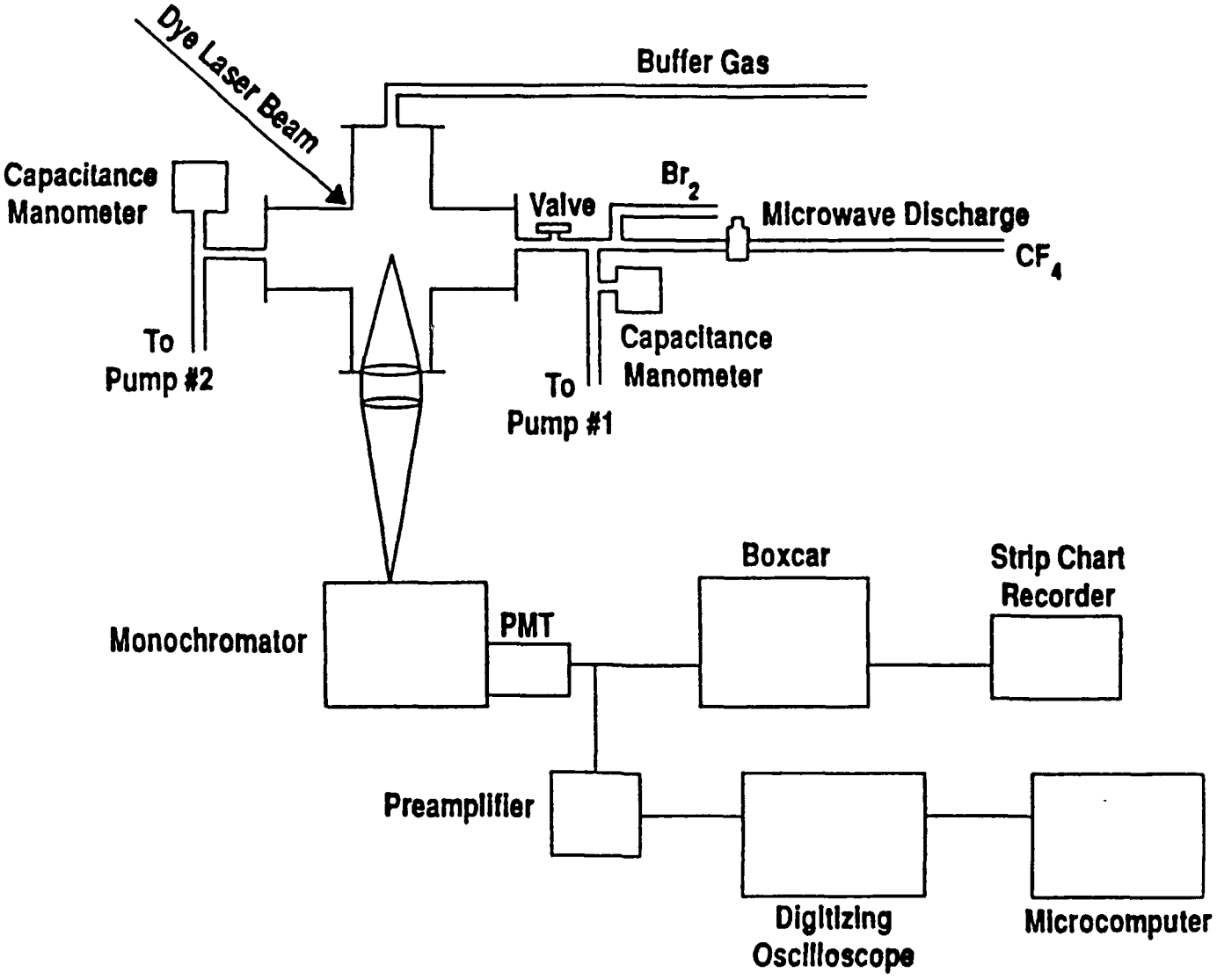

Figure 4. Experimental Apparatus[6]

The F atoms are created from the dissociation of Airco 99.7% CF_4 by a Opthos 100 watt, 2450 MHz microwave discharge that dissociates approximately 1% of the CF_4 into fluorine atoms.[6] This is then combined with the Br_2 which flows by vapor pressure from Spectrum Chemical 99.5% liquid Br_2. BrF(X) is produced at pressures of greater than 1 torr and a ball valve is used to reduce and vary the pressure inside the cell. Nupro S-series valves are used to control the gas flows, however pressure, not flow, is the relevant data.

The fluorescence cell consists of a six-way cross, 7.2 cm in diameter and 20 cm in length, made of stainless steel with pyrex windows. Along the z-axis is the laser pathway. The laser is reflected into the chamber through a Brewster angled window, travels straight through and exits through another Brewster angled window which reduces reflection and scatter. The BrF flow is along the y-axis. It enters through the ball valve at the right and exits to the pump at the left. Along the third axis is the observation window at one end and the input for the buffer gases used for the energy transfer studies at the other.

BrF is produced at high pressures to maximize the amount of BrF and to prevent back pressure due to high chamber pressures from disrupting the conditions of production. However, increased pressure and low flow rates in the production area disrupted the efficiency of the microwave discharge. For studies where low chamber pressure were used, BrF was produced at pressures of about 1 torr. For the studies where higher chamber pressures were used, the BrF was produced at pressures up to 3 torr.

The cell was evacuated to approximately 3 mtorr with a Sargent-Welsh model 1462, 25 l/m pump. Because of the large difference in BrF(X) production pressures and the cell pressures, another similar pump was used prior to the cell to discharge excess mix. An MKS model 122a, 10 torr head capacitance manometer is used prior to the chamber to measure the mix pressures. An MKS model 390, 1 torr head capacitance manometer is used to measure pressures ranging from 50 to 600 mtorr in the fluorescence cell. For the energy transfer studies involving the rare gases, the 10 torr Baratron was moved to the chamber to measure the higher chamber pressures that were required. The leak plus outgassing rates for the fluorescence cell were approximately 1 mtorr/hour.

Research grade (99.999%) rare gases, He, Ne, Ar, Kr, and Xe, bottled by Airco were used as buffer gases in these energy transfer studies. The flow was adjusted through a Nupro leak valve and injected directly into the chamber. The buffer gases did not interact with the mix gases, except in the chamber, to avoid any variations in the mix concentrations due to the changing buffer gas concentration. However, in some cases, the flow was disrupted by the buffer gases as explained in section 4.2.1 and Appendix B.

3.2 Excitation System

Ground state BrF was excited to a specific ro-vibrational level within the B state in the fluorescence cell by a Spectra-Physics PDL-3 pulsed dye laser which was pumped by a Quanta-Ray DCR-3 pulsed ND:YAG laser. Selected ro-vibrational levels in BrF(B) were populated by

tuning the dye laser to a suitable absorption line in the B ← X system. The dye laser produced pulses of 10 nanosecond pulse width at 10 mJ/pulse and a repetition rate of 20 Hz. 1000 to 4000 laser pulses were averaged for each measurement. The beam was directed through the center of the fluorescence cell by a system of mirrors. The convergence of the beam was manually adjusted so that it would be approximately one mm diameter while traversing the chamber.

The v'= 2 (P27 of ^{81}BrF), v'= 5 (P11, R15 of ^{79}BrF and P10, R14 of ^{81}BrF), and v'= 6 (P21 of ^{81}BrF) transitions to BrF(B) were pumped from the v" = 0 band of the ground state, with wavelengths of 5331.3Å, 5044.3Å and 4978.4Å respectively. These transitions were chosen due to the range in v' to study below the pre-dissociation level, as well as the strong Franck-Condon factors and relative isolation of the bands. Pre-dissociation begins to occur at v'= 7 and BrF is totally dissociated at v'= 8.[17] The 6-0, 5-0, and 2-0 bands were chosen to give a broad range of vibrational energies to study. Coumarin 500 dye by Exciton was used for the entire study because it has the necessary wavelength range and power required.

3.3 Fluorescence Detection System

The detection system consisted of an Instruments SA model HR60 0.64m monochromator with 1200 grove/mm grating, and an RCA C31034 photomultiplier tube (PMT). A lens focusing arrangement was placed between the window of the cell and the monochromator to increase the signal strength. A 10 cm focal length lens was approximately focused on

the laser beam centered in the cell. A second lens (f = 25 cm) focused the parallel rays from the first lens onto the entrance slit of the monochromator. Entrance and exit slits of 1 mm were used which provided a resolution of 22.4Å.[6]

The signal was preamplified by a Princeton Applied Research Corporation (PARC) model 115 preamplifier and displayed on a LeCroy 9450, 350 MHz oscilloscope/data processor. The LeCroy was pre-triggered by the laser with an approximate 10% pre-trigger. Decay profiles of 10 to 100 μsec were measured with up to 4000 shot averaging. This decay profile was then downloaded to a Zenith Z-248 computer for subsequent data analysis. A PARC model 160 boxcar integrator and a strip chart recorder were used to record the vibrational spectrum.

3.4 Experimental Procedure

During the self transfer studies the basic procedure involved measuring the signal of the laser induced fluorescence of the BrF, then subtracting the noise measured with only a residual background (i.e. no BrF mix). With a pretrigger from the laser, the LeCroy averaged the signal over 1000 to 4000 shots to improve the signal to noise ratio. This was done at ten different mix pressures in the fluorescence cell from about 750 mtorr to as low as measurable, usually about 70 mtorr. This procedure was repeated at each vibrational level examined and for each vibrational level pumped. Table I shows what vibrational states were monitored.

Table I. Gas, Pump Level and Transitions Observed

gas	pump transition v" – v'	observed transition v' – v"
mix	0 – 6	6 – 6
		5 – 2
		4 – 3
		3 – 3
		2 – 9
		1 – 6
		0 – 8
	0 – 2	3 – 4
		2 – 9
		1 – 6
		0 – 8
Argon	0 – 6	5 – 2
		3 – 3
	0 – 5	6 – 6
		4 – 3
		2 – 9
	0 – 2	1 – 6
Helium	0 – 5	4 – 3
		2 – 9
	0 – 2	1 – 6
Neon	0 – 5	4 – 3
Krypton	0 – 5	4 – 3
Xenon	0 – 5	4 – 3

The vibrational transfer studies involving the rare gases had a slightly different procedure. Again, about ten different measurements similar to above were made, however, the pressure of the buffer gas was varied while keeping the partial pressure of the BrF mix constant. This partial pressure was made as low as possible, approximately 100 mtorr, while maintaining a strong signal. The buffer gas pressure was varied from no buffer gas to approximately 2 torr total pressure. Again, this procedure was repeated at each vibrational level examined (see Table I).

3.5 Experimental Calculations

As stated above, the resolution of the monochromator was 22.4Å. As can be seen in Figure 26 of Appendix A, this resolution can cover numerous vibrational transitions. The resolution of the monochromator must be large enough to obtain a good quality signal, but this often means that more then one transition is inadvertently observed. Transitions to be observed in this research were selected by their strong Franck–Condon factors and their relative isolation from other strong transitions, as can be seen in Figure 26. However, no observed transition was completely isolated, other transitions always overlapped the selected transition and this had to be accounted for.

If the intensity versus wavelength of a vibrational band is modelled by a triangle as shown in Figure 5, the effective intensity at a wavelength other than the bandhead can be determined. The effective intensity is simply

$$I_{eff} = \begin{cases} \left[1 - \frac{\lambda_{BH} - \lambda_{obs}}{100}\right] \times N_{v'} q_{v'v''} & \lambda_{BH} \leq \lambda_{obs} < \lambda_{BH} + 100\text{Å} \\ \left[1 - \frac{\lambda_{obs} - \lambda_{BH}}{30}\right] \times N_{v'} q_{v'v''} & \lambda_{BH} - 30\text{Å} < \lambda_{obs} < \lambda_{BH} \\ 0 & \textit{otherwise} \end{cases} \quad (16)$$

where:

λ_{BH} is the bandhead frequency determined by (1) for either the observed transition or an overlapping transition

λ_{obs} is the setting of the monochromator

$N_{v'}$ is the number density in the v' level

$q_{v'v''}$ is the Franck-Condon factor for the transition

And the total intensity observed at a particular wavelength is the sum of all effective intensities within the resolution of the monochromator at the observation wavelength. The width of the triangles were

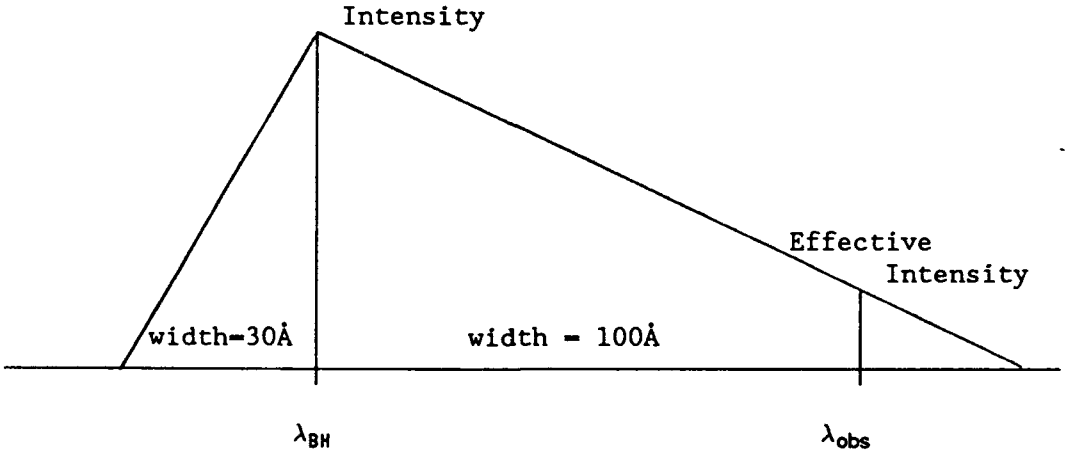

Figure 5. Triangle overlap fractions

determined by fitting with the Montroll-Shuler model to a best fit of the data. The best fits were found for triangle widths of 100Å on the long wavelength side and 30Å on the short wavelength side. These values for triangle widths and overlaps were then used throughout this study.

We can consider the expression in brackets in equation 16 multiplied by the Franck-Condon factor as an effective Franck-Condon factor. Each transition observed (see Table I) will have some overlap from other transitions, so an effective Franck-Condon factor is found for each.[3] Table II shows by each transition the observed wavelength (i.e. the monochromator setting), the bandhead wavelength, the Franck-Condon factor and an effective Franck-Condon factor for both the observed transition and overlapping transitions. The percent of emission from an overlap to the observed transition ranged from a low of 7% for the v'= 3 transition to a high of 71% for the v'= 6 transition.

A major step in the data reduction process was fitting the Montroll-Shuler model to a plot of the data, at each measured pressure. A PASCAL program, written by Melton,[14] was used to fit the model to the data. The output of the program, along with the data points for the Montroll-Shuler curve fit, was an estimate of the fundamental $k_v(1,0)$ rate coefficient. This value, multiplied by the concentration of the mix was then plotted versus concentration using a Stern-Volmer technique. The slope of a linear least squares fit to these points provided the fundamental rate coefficient for that transition.

Table II. Transition Wavelengths and Franck-Condon Factors

TRANSITION (v' - v")	OBSERVED WAVELENGTH (Å)	BANDHEAD WAVELENGTH (Å)	FRANCK-CONDON FACTOR	EFFECTIVE FCF
6 - 6	6135	6137	0.03594	0.033544
1 - 3		6051.7	0.02554	0.004265
2 - 4		6156.7	0.08611	0.023824
5 - 2	5398	5396.5	0.06505	0.064074
3 - 1		5396.5	0.01128	0.011111
6 - 2		5308.7	0.06332	0.006775
4 - 3	5695.5	5694	0.07397	0.072545
2 - 2		5704.8	0.02086	0.014393
7 - 4		5605.6	0.00887	0.000896
3 - 3	5806.1	5804.4	0.0738	0.072545
5 - 4		5799.1	0.00918	0.008537
7 - 5		5811.4	0.03774	0.031073
3 - 4	6028.2	6028.2	0.07635	0.07635
1 - 3		6051.7	0.02554	0.005534
0 - 2		5951.2	0.00145	0.000333
2 - 9	7635.5	7597	0.06087	0.037435
4 - 10		7546.1	0.03017	0.003198
1 - 6	6887	6835.6	0.10795	0.052464
3 - 7		6794.8	0.02489	0.001941
6 - 9		6910.5	0.03809	0.008253
0 - 8	7685	7670.4	0.15671	0.133830
7 - 12		7686.6	0.01554	0.014711
2 - 9		7597	0.06087	0.007304

Following Landau-Teller, each fundamental rate coefficient was multiplied by the vibrational quantum number of the transition for which it was found. This was plotted versus the quantum number to determine the adequacy of the Landau-Teller theory for BrF. A linear least-squares fit was made to find the average fundamental rate coefficient for that pump level.

IV. Results and Discussion

The experimental results can be conveniently divided into two parts. First, vibrational transfer for the mix was measured for the various levels as shown in Table I. This was done in detail, to include a variety of different pump and observation levels. The purpose was to characterize the BrF mix, which includes BrF(X), Br_2, F, CF_4 and minor amounts of CF_3 and C_2F_6, and determine how well it obeys the models presented above. After this, then vibrational transfer with other gases could be measured. This was done in detail for the first buffer gas studied, argon, but in less detail for helium and even less for the remaining rare gases. As it was demonstrated that the Montroll-Shuler model was fairly correct in predicting behavior, less detailed study was necessary.

4.1 Self-Transfer

The self-transfer study was performed over three different pump levels which were chosen to span the stable portion of BrF(B) and had strong Franck-Condon factors. Melton[6] performed a preliminary study by pumping v'= 5 and observing transitions involving levels v'= 6 through 0. The current study additionally pumped v'= 6 observing levels v'= 6 through 0, and pumped v'= 2 observing levels v'= 3 through 0 (Table I).

4.1.1 Excitation of v' = 6. Figure 6 gives an overview of the effect of vibrational transfer. Shown in Figure 6 is a superimposed fluorescence trace from various vibrational levels, v'= 6 through 0, after pumping v'= 6. The trace from v'= 6 is a simple exponential decay. The fluorescence from the other vibrational levels increases as the population moves into that level and then decreases as the population decays. As the vibrational level gets further from the pump level, the signal decreases and, more importantly, the peak of fluorescence moves out further in time as it takes longer for the population to reach that particular vibrational level. From this type of data, vibrational rate coefficients can be determined.

Figures 7 - 13 show samples of data with superimposed Montroll-Shuler fits for pump v'= 6, observing v'= 6 through 0 respectively. This data were taken at the pressures shown, however for every case, approximately ten different measurements were taken at different pressures. The Montroll-Shuler model then fits to the data with an output of the fundamental rate coefficient, $k_v(1,0)$, for that transition, at that pressure.

4.1.1.1. Montroll-Shuler Model. From Figures 7 - 13, it can be seen that the Montroll-Shuler model fits fairly well with these transitions. The early transitions, v'= 6 through 3 have excellent fit, all within the noise of the signal. The transitions with the poorest fits are from v'= 2, 1, and 0, shown in Figures 11 - 13. Multi-quantum transfer is a possible explanation for these poor fits,

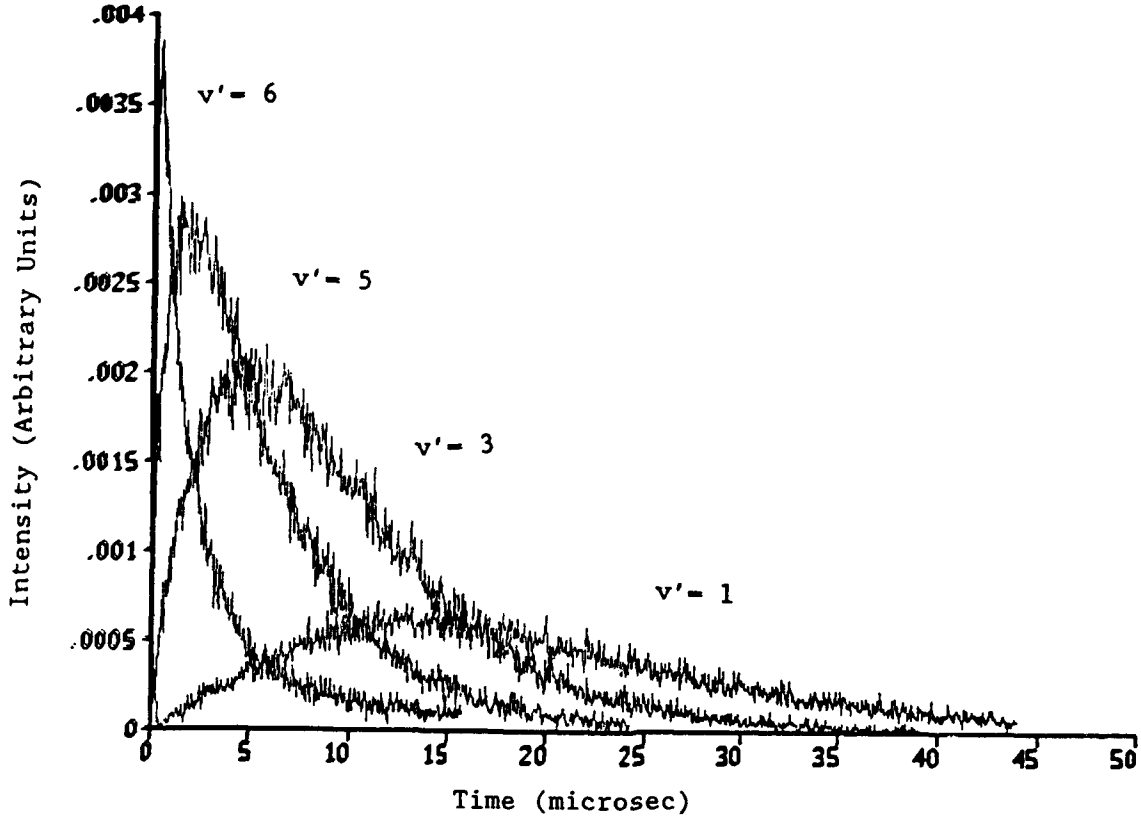

Figure 6. Demonstration of Vibrational Transfer

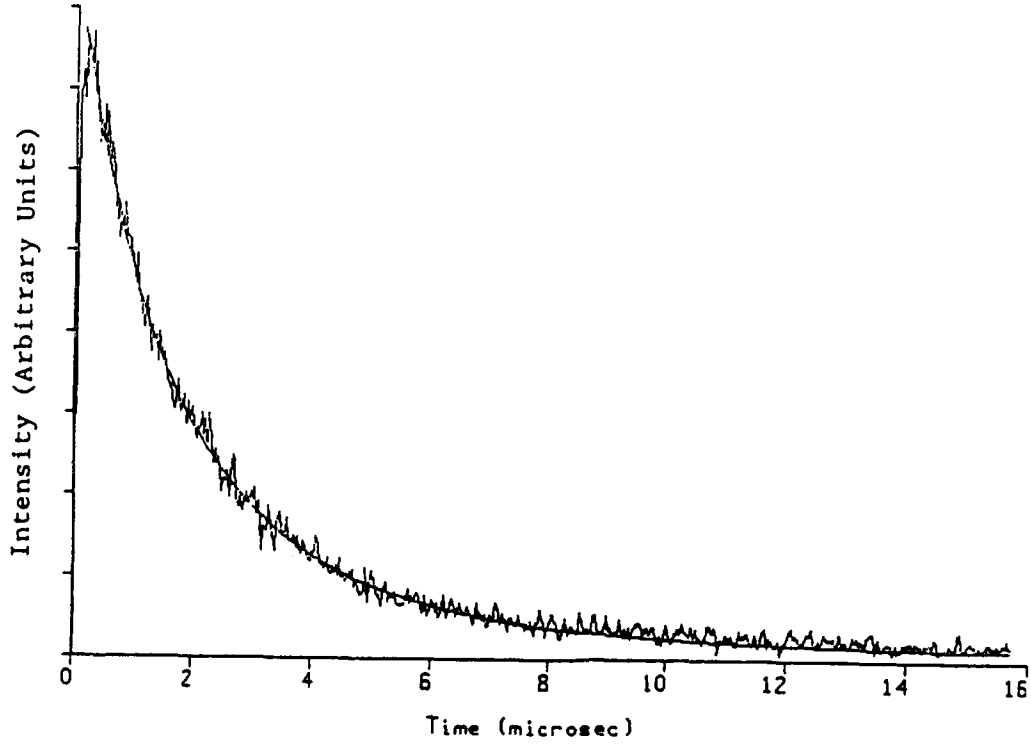

Figure 7. Montroll-Shuler fit to pump v'= 6, observe v'= 6 (6135Å), pressure = 523.0 mTorr data

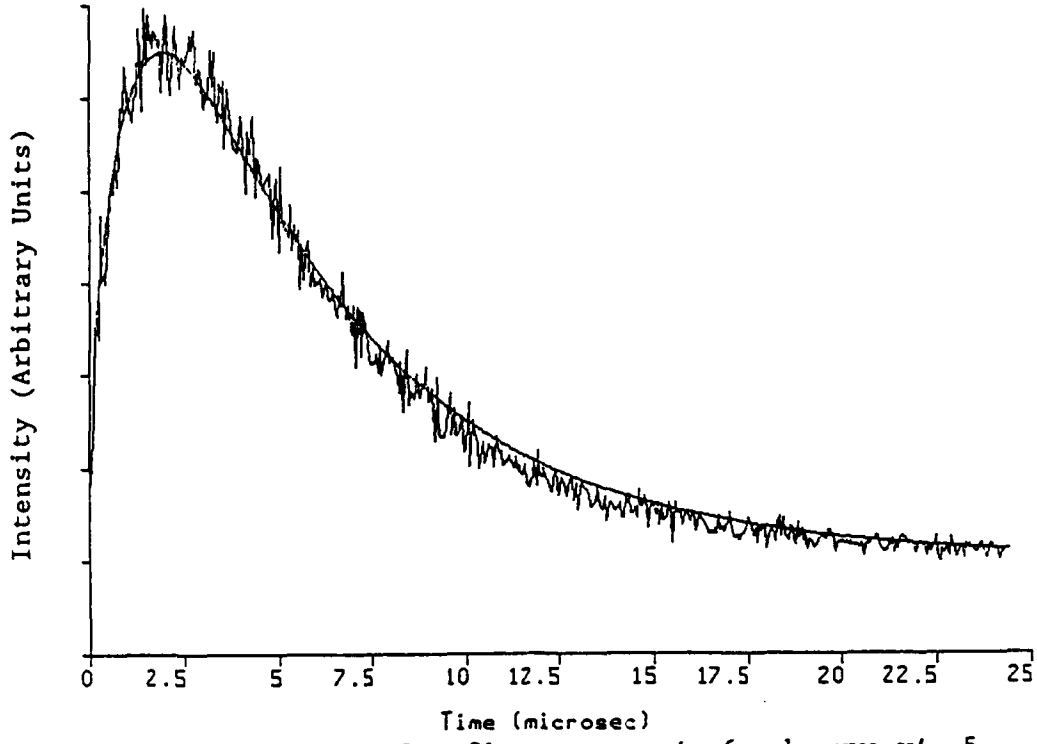

Figure 8. Montroll-Shuler fit to pump v'= 6, observe v'= 5 (5348Å), pressure = 518.8 mTorr data

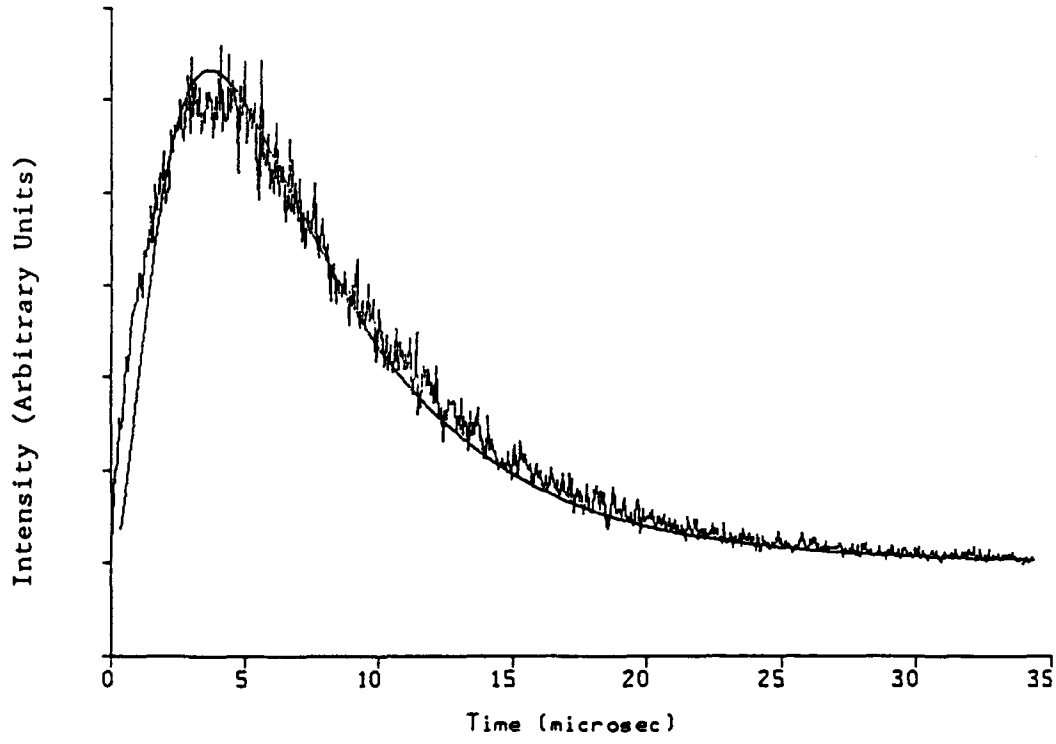

Figure 9. Montroll-Shuler fit to pump v'= 6, observe v'= 4 (5695.5Å), pressure = 522.7 mTorr data

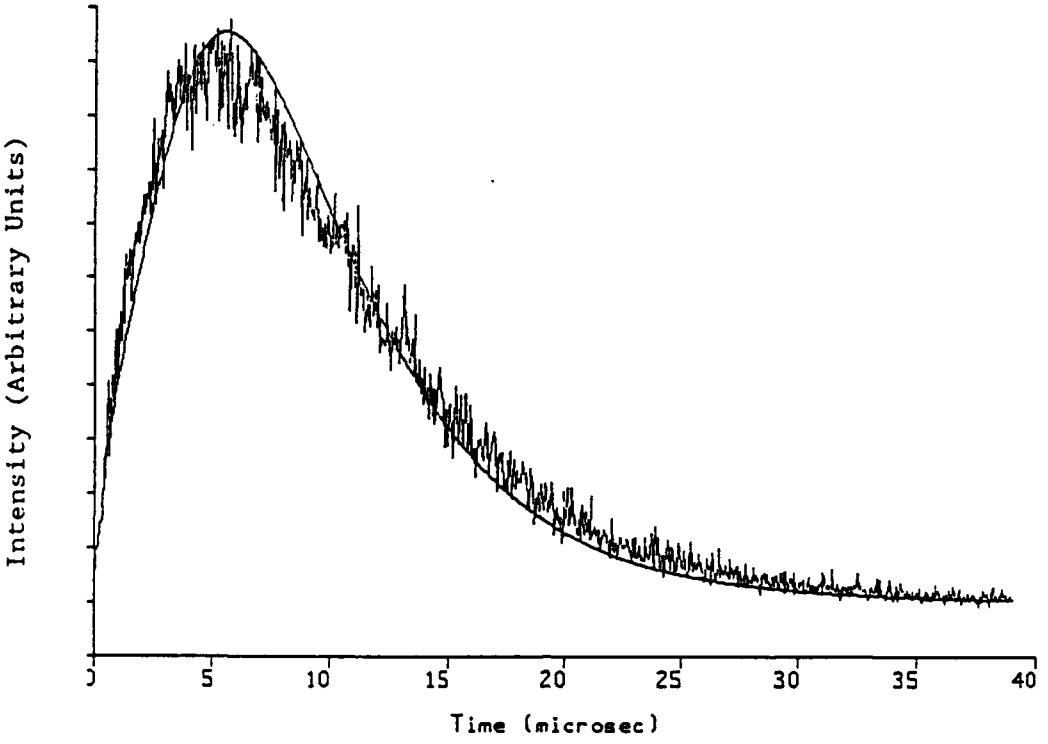

Figure 10. Montroll-Shuler fit to pump v'= 6, observe v'= 3 (5806.1Å), pressure = 598.2 mTorr data

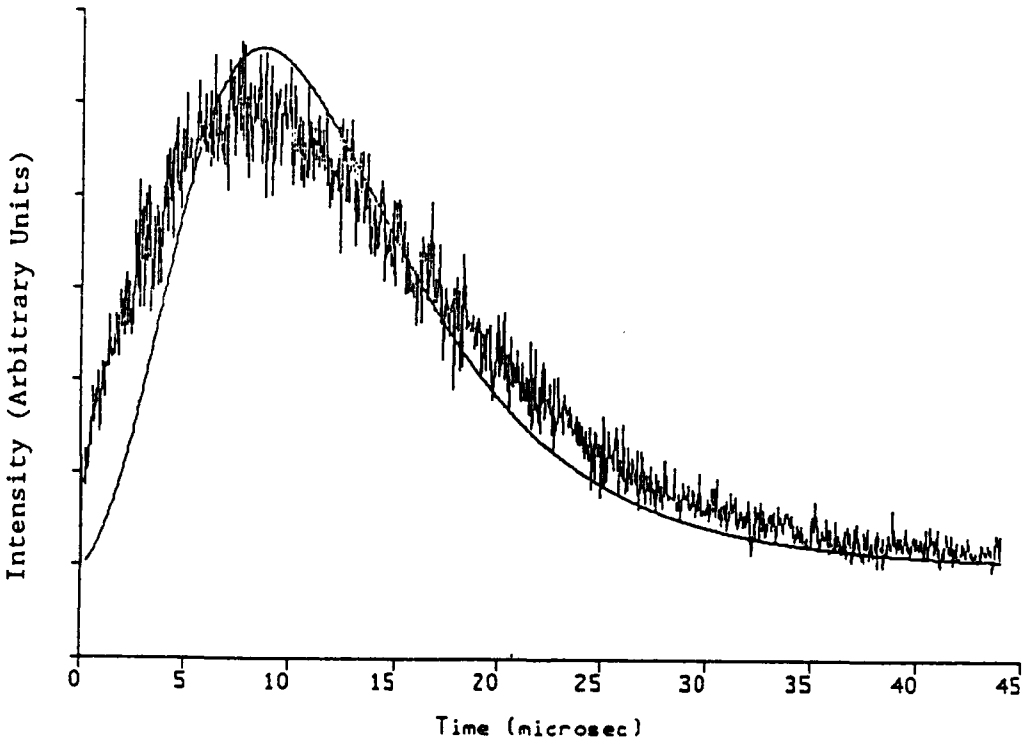

Figure 11. Montroll-Shuler fit to pump v'= 6, observe v'= 2 (7635.5Å), pressure = 522.9 mTorr data

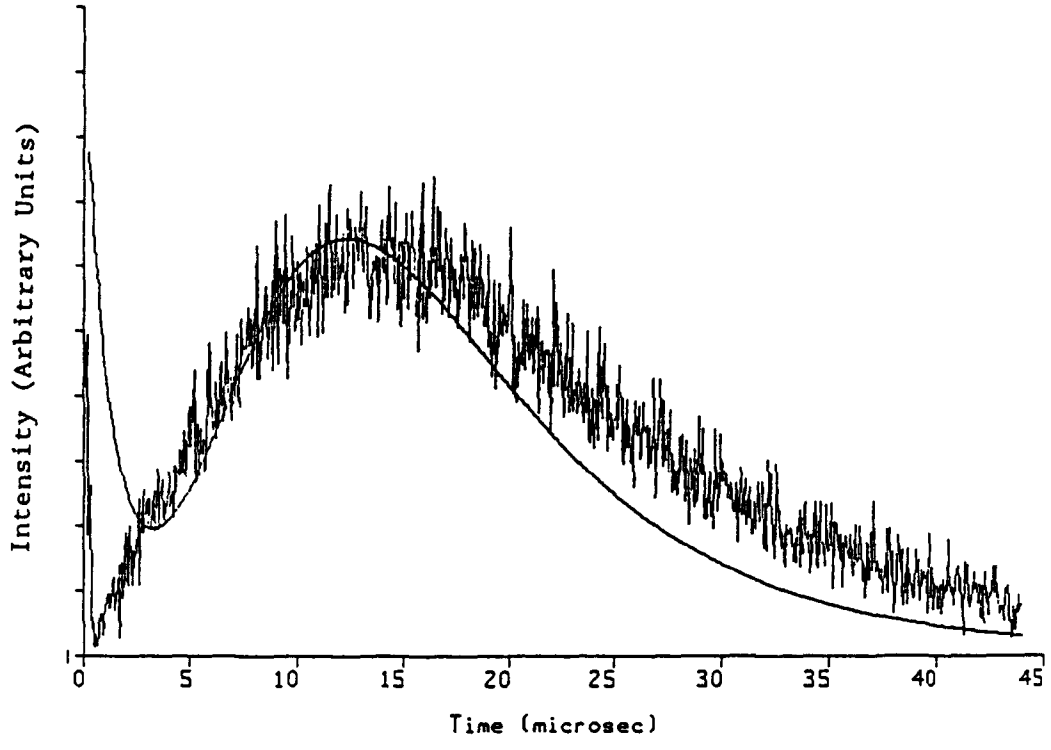

Figure 12. Montroll-Shuler fit to pump v'= 6, observe v'= 1 (6887.0Å), pressure = 602.9 mTorr data

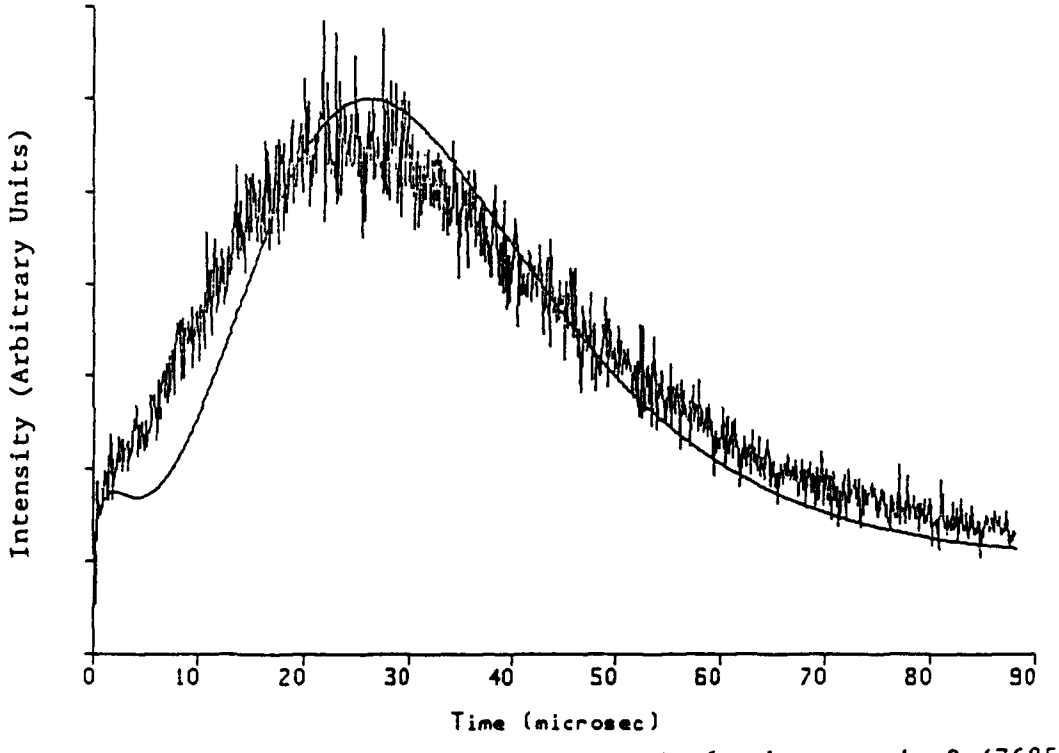

Figure 13. Montroll-Shuler fit to pump v'= 6, observe v'= 0 (7685.0Å), pressure = 531.2 mTorr data

because the Montroll-Shuler model assumes vibrational transfer of $\Delta v' = \pm 1$ only. Multi-quantum transfer would reveal itself by a slow trend with decreasing v' of a stronger intensity earlier than predicted by the Montroll-Shuler model. Another explanation of the poor fit to the model is the overlap fractions used in the model. Appendix B has a detailed discussion of overlap fractions and possible systematic errors.

4.1.1.2 Stern-Volmer Plots. The fundamental rate coefficients produced by the Montroll-Shuler model at each pressure are multiplied by the mix concentration and plotted versus the concentration using a Stern-Volmer technique. This is done for each transition examined and produces an average $k_v(1,0)$ from the slope. Figure 14 shows an example of this for the decay from the initially populated $v' = 6$ state. For all transitions the linearity is good but the intercept, which should ideally be zero, is often positive and greater then it's uncertainty. Possible explanations of this include the BrF(B) lifetime being dependent on v', incorrect overlap fractions or predissociation. This will be further discussed in Appendix B. Table III shows the fundamental rate coefficient, $k_v(1,0)$, for each pump $v' = 6$ transition observed found from a Stern-Volmer plot. The error quoted was found from the standard deviation of the slope. The weighted average of rate coefficients for pump 6 transitions is $(4.6 \pm .6) \times 10^{-12}$ $cm^3/(molecules \cdot sec)$.

Table III. Fundamental Rate Coefficients for Pump 6 Transitions

v'	Rate Coefficient (10^{-12} cm^3/molecule·sec)
6	4.180 ± .06
5	3.864 ± .07
4	5.105 ± .15
3	5.036 ± .28
2	5.454 ± .06
1	4.855 ± .07
0	4.147 ± .34
Avg $k_v(1,0)$ = 4.6 ± .6	

4.1.1.3 Landau-Teller Scaling. From the fundamental rate coefficients for each transition, the Landau-Teller model can be evaluated. Figure 15 demonstrates this by plotting the product of the rate coefficient and quantum number versus quantum number. The plot shows good linearity with little evidence of curvature; the linear trend of rate coefficient $k(v \rightarrow v-1)$ with vibrational quantum number is verified. The Landau-Teller model can be considered valid at this point for BrF and vibrational transfer can be described by a single, fundamental rate coefficient, $k(v',v'-1) = v'k_v(1,0) = (4.6 \pm .6) \times 10^{-12}$ cm^3/(molecules•sec).

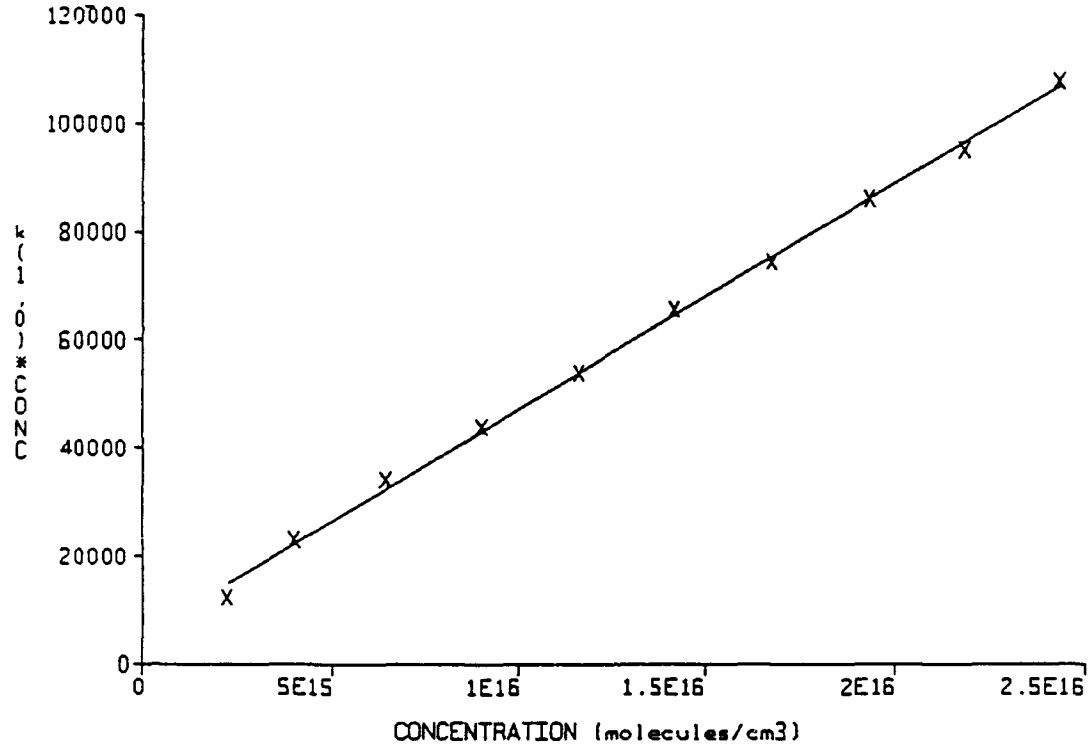

Figure 14. Stern-Volmer plot of pump v'= 6, observe v' = 6 data

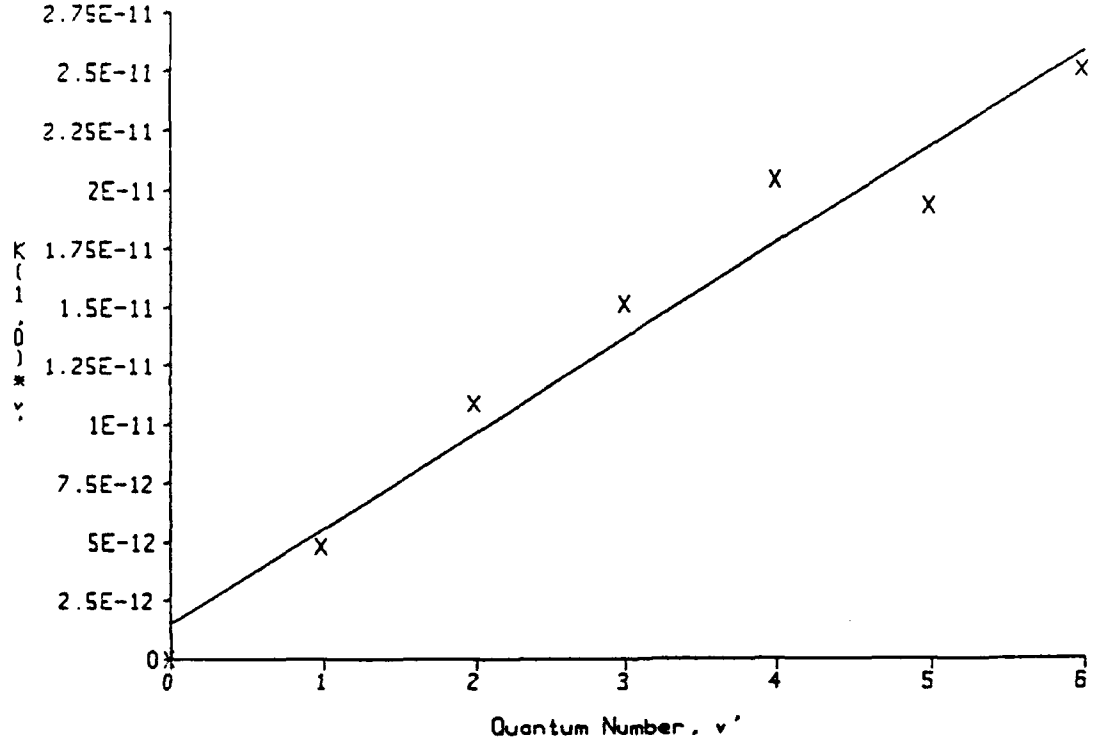

Figure 15. Landau-Teller fit to pump v'= 6 data

4.1.2 Excitation of v' = 5. The study of vibrational transfer by pumping v'= 5 and observing transitions v'= 6 through v'= 0 was performed by Melton.[6] His experiment used the same apparatus as this study, and comparisons between the two should be valid. Table IV shows the fundamental rate coefficients by transition. Melton found that BrF obeyed Landau-Teller with a fundamental rate coefficient of $k_v(1,0)$ = (3.5 ± .6) x 10^{-12} cm^3/(molecule·sec). This is lower than the rate coefficient found for the pump v'= 6 level found in this study, but the error bounds overlap. The different values might be caused by the different overlap fractions used. This will be further explained in Appendix B.

Table IV. Fundamental Rate Coefficients for Pump 5 Transitions[6]

v'	Rate Coefficient ($10^{-12}cm^3$/molecule·sec)
6	2.8 ± .1
5	4.5 ± .2
4	3.54 ± .03
3	4.0 ± .1
2	3.77 ± .06
1	2.55 ± .06
0	3.7 ± .1
Avg $k_v(1,0)$ = 3.5 ± .6	

4.1.3 Excitation of v' = 2. Following the pumping of vibrational level v'= 6 and observing transitions from 6 through 0, level v'= 2 was pumped and transitions from v'= 3 through 0 were observed. Figures 16 - 19 show the data with Montroll-Shuler fits.

4.1.3.1 Montroll-Shuler Model. As above for the pumping v' = 6, the Montroll-Shuler model has good fits to the data for all transition levels. For the v' = 2 to v" = 9 transition (Figure 17), the model was fit to the data which came >1 μsec after the laser pulse. The data before 1 μsec showed a very high intensity with a very fast dropoff. This was assumed to be fluorescence from Br_2^*, which is produced by exciting Br_2 at the pump v' = 2 laser wavelength. The poor fit of the 0 - 8 transition is, again, possibly caused by poor overlap fractions or multi-quantum transitions (see Appendix B).

4.1.3.2 Stern-Volmer Plots. A Stern-Volmer technique is again used at each transition to produce a rate coefficient. Figure 20 shows an example from the 2 - 1 transition. In all cases the linearity and the intercepts were good. Table V gives the rate coefficient and standard deviations found from each transition. Also given is the weighted average of these rate coefficients.

4.1.3.3 Landau-Teller Scaling. The Landau-Teller model is again evaluated by plotting the product of the rate coefficient and quantum number versus the quantum number. Figure 21 shows this plot and

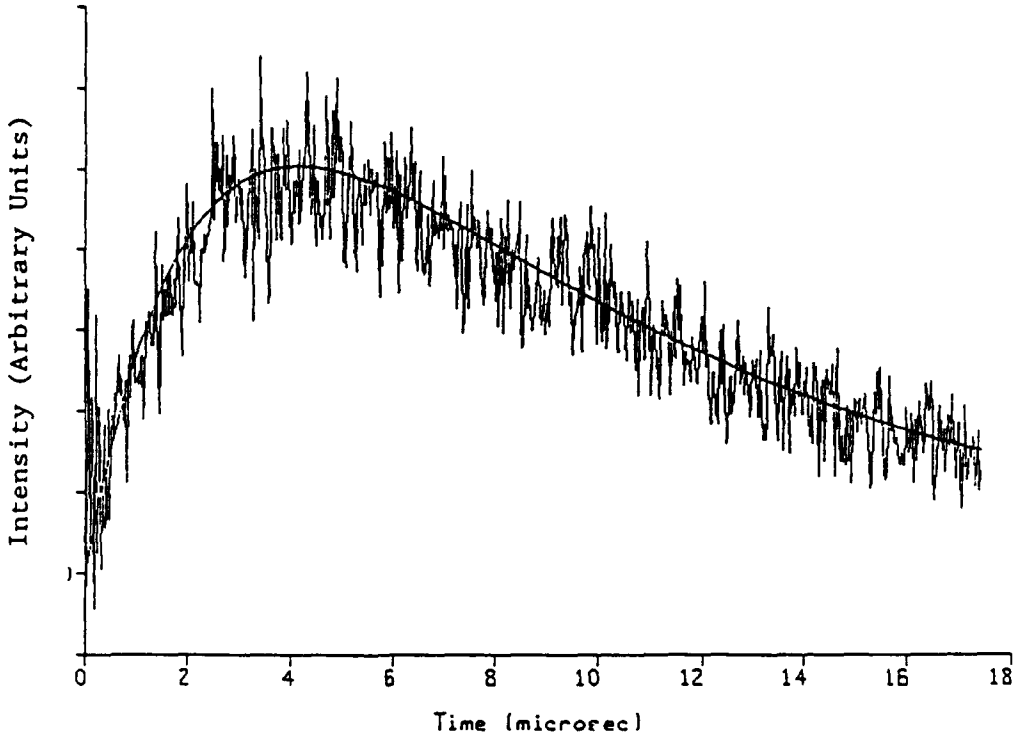

Figure 16. Montroll-Shuler fit to pump v'= 2, observe v'= 3 (6028.2Å), pressure = 425.1 mTorr data

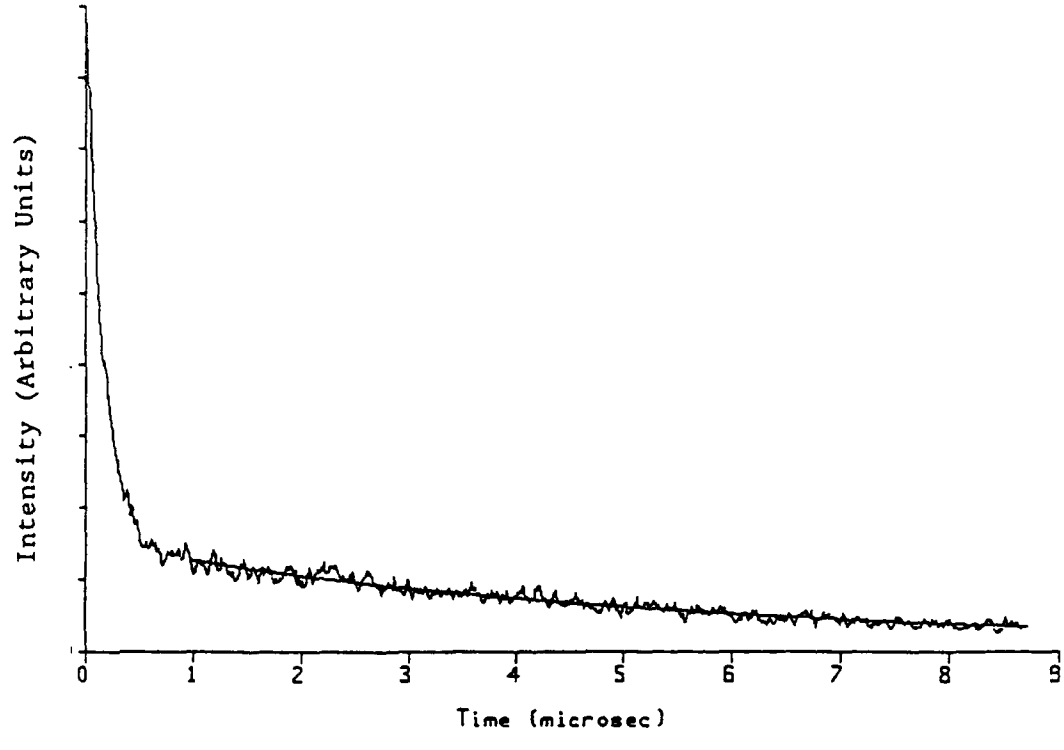

Figure 17. Montroll-Shuler fit to pump v'= 2, observe v'= 2 (7635.5Å), pressure = 420.8 mTorr data

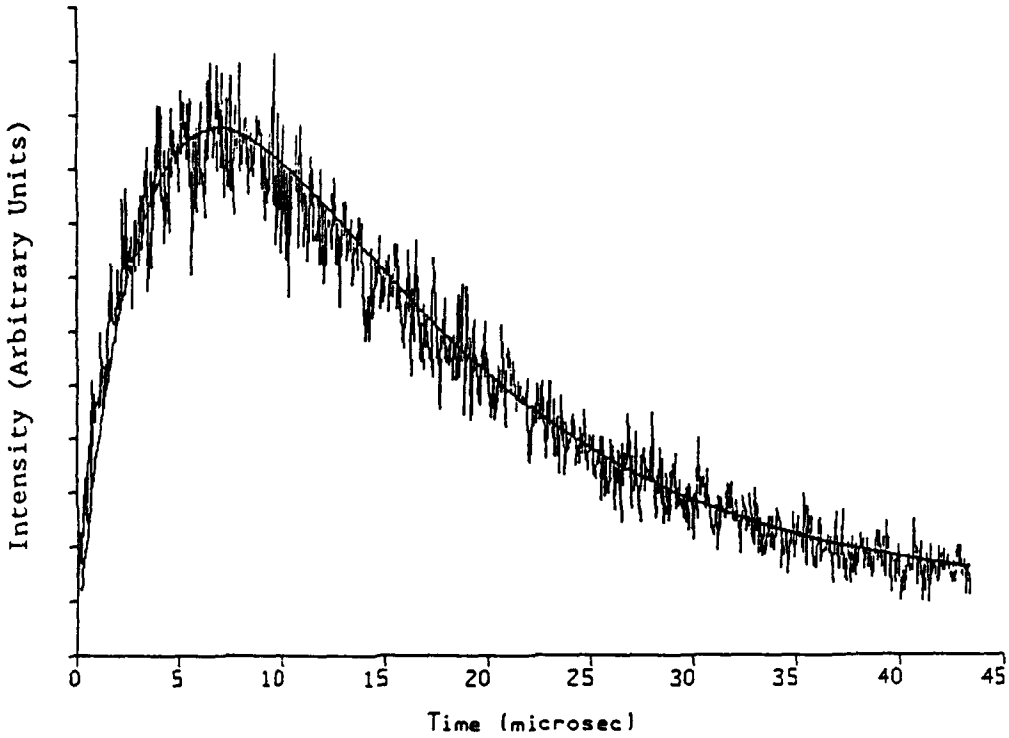

Figure 18. Montroll-Shuler fit to pump v'= 2, observe v'= 1 (6887.0Å), pressure = 420.4 mTorr data

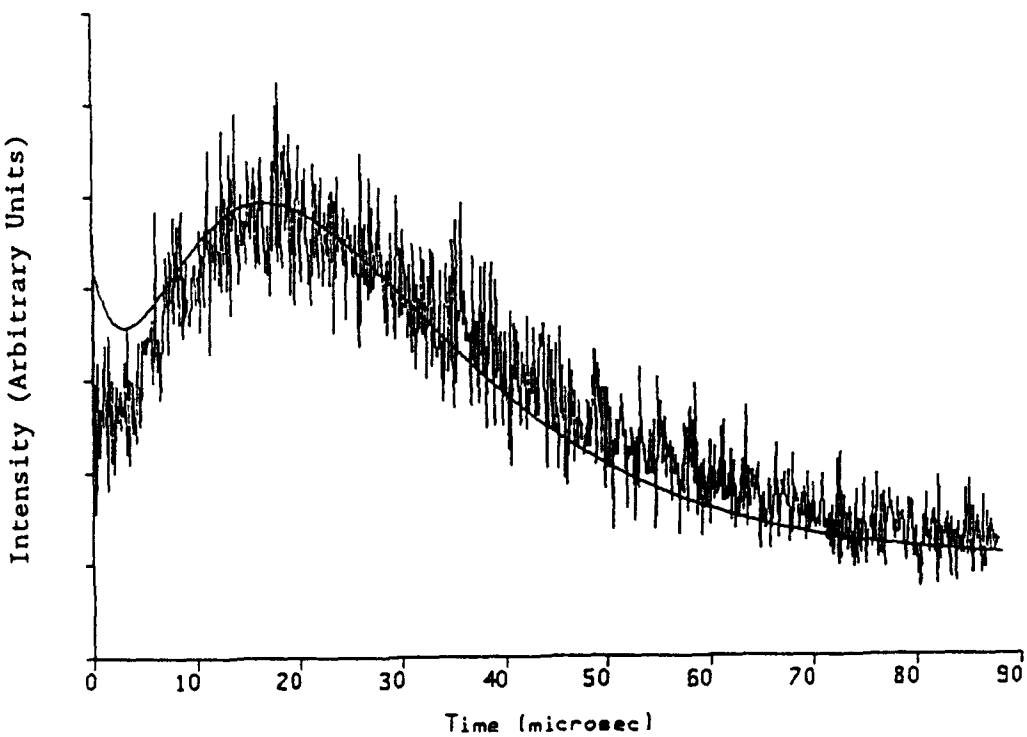

Figure 19. Montroll-Shuler fit to pump v'= 2, observe v'= 0 (7685.0Å), pressure = 485.2 mTorr data

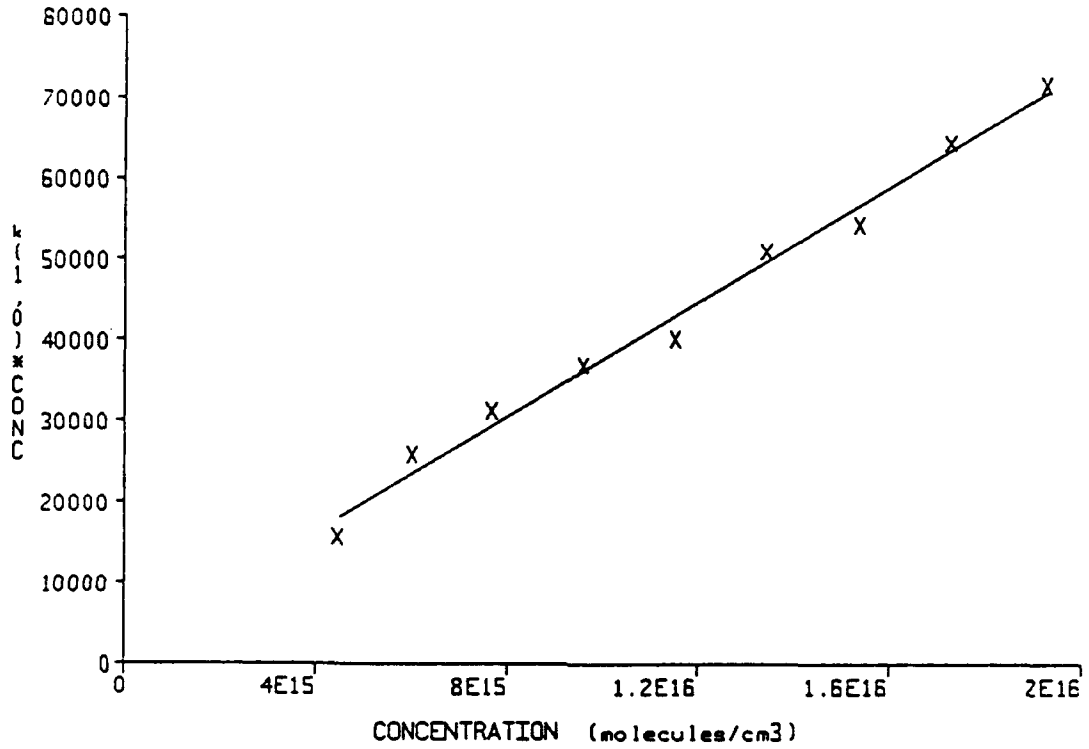

Figure 20. Stern-Volmer plot of pump v'= 2, observe v' = 1 data

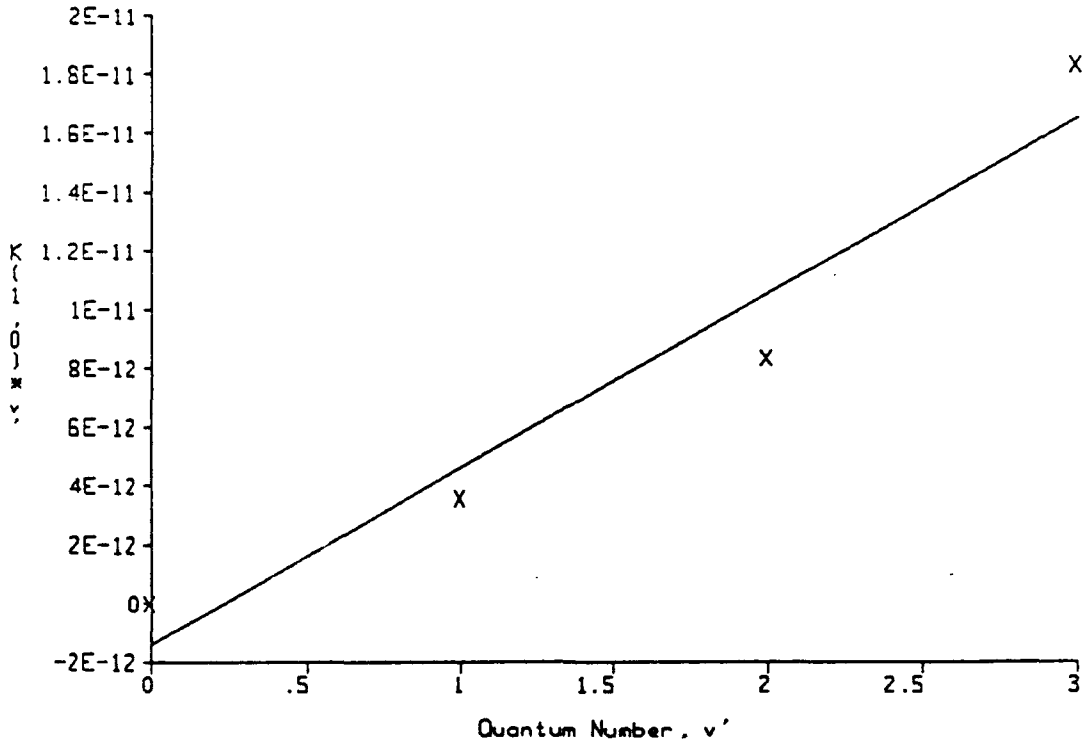

Figure 21. Landau-Teller fit to pump v'= 2 data

demonstrates the fairly good linearity. However, as opposed to the pump 6 data, this data shows some curvature; the rate coefficients have a definite trend with quantum number. Table V shows that the rate coefficients increase with vibrational level. This is difficult to explain as being a real effect because Landau-Teller scaling worked so well at $v' = 6$, and $v' = 5$, which are higher on the potential curve. A possible explanation could be the signal to noise ratio is much worse for the pump $v' = 2$ transitions due to the smaller Franck-Condon factor.

Table V. Fundamental Rate Coefficients for Pump 2 Transitions

v'	Rate Coefficient ($10^{-12}cm^3$/molecule·sec)
3	6.121 ± .25
2	4.189 ± .2
1	3.564 ± .15
0	2.272 ± .25
Avg $k_v(1,0) = 3.9 \pm 1.4$	

4.1.5 Comparison to the Other Interhalogens. Averaging the pump 6, pump 5 and pump 2 data yields an average fundamental rate coefficient of $k_v(1,0) = (4.0 \pm .5)\ x10^{-12}$ $cm^3/(molecules \cdot sec)$. This is comparable to the $v_i = 3$ to $v_f = 2$ rate coefficient, $k_v(3,2) = (5.8 \pm .5)\ x10^{-12}$ $cm^3/(molecules \cdot sec)$, for IF with F_2 as the collision partner.[4] BrCl has

a fundamental rate coefficient of 1.3 $x10^{-11}$ $cm^3/(molecules \cdot sec)$ for Cl as the collision partner. BrF is in the same order of magnitude as these other interhalogens.

4.2 Vibrational Transfer by the Rare Gases

Vibrational transfer study with the rare gases was performed following the self-transfer studies above. The rare gases were chosen as buffer gases because of their simpler structure (i.e. no vibrational-to-vibrational or vibrational-to-rotational transfer involved), and for comparison to previous work. Argon was studied in depth by pumping levels v' = 6, 5, and 2 and observing transitions involving levels v' = 1 through 6. Helium was next examined in lesser detail by pumping v' = 5 and 2 and observing transitions from v' = 4, 2, and 1. Rate coefficients were found for neon, krypton, and xenon by simply pumping v' = 5 and examining the transition from v' = 4.

4.2.1 Argon Argon was studied in depth because it is in middle of the rare gases by mass and atomic number. As noted in Section 3, the study of vibrational transfer with the rare gases used essentially the same procedure as for self-transfer except relatively high pressures were required for the buffer gases for a noticeable change in signal. Also, the lowest possible mix pressure was used to assure that the majority of BrF(B) collisions involved collisions with the buffer gas, yet keeping a high enough pressure for an adequate signal.

As above for self-transfer, the data reduction involved fitting the data to the Montroll-Shuler model to produce a rate coefficient. The fits were excellent at each vibrational level observed; no poor fits were found which might imply multi-quantum transfers. As before, the rate coefficients were plotted using a Stern-Volmer technique to obtain the fundamental rate coefficient, $k_v(1,0)$. A few of the intercepts of these plots were highly negative which will be discussed in Appendix B. Table VI presents these fundamental rate coefficients by observed transition.

As seen from Table VI and Figure 22, a Landau-Teller fit, the Landau-Teller model does not seem to correctly predict the behavior of vibrational transfer with argon. However, when correlating the high background pressure mixes and the Stern-Volmer plots with bad intercepts, these transitions also have rate coefficients that are lower than average and the largest error bounds. High background mix pressure can disrupt the flow through the system and create a scenario where the rate coefficient will be measured lower than it actually is. Appendix B will explain this in more detail. Neglecting the worst of these, the $v' = 6$ transition, yields a good fit to Landau-Teller scaling (see Figure 23), with an average fundamental rate coefficient, $k_v(1,0) = (9.7 \pm 5) \times 10^{-13}$ $cm^3/(molecules \cdot sec)$ that is consistent with the other data but with an approximately 50% error bound.

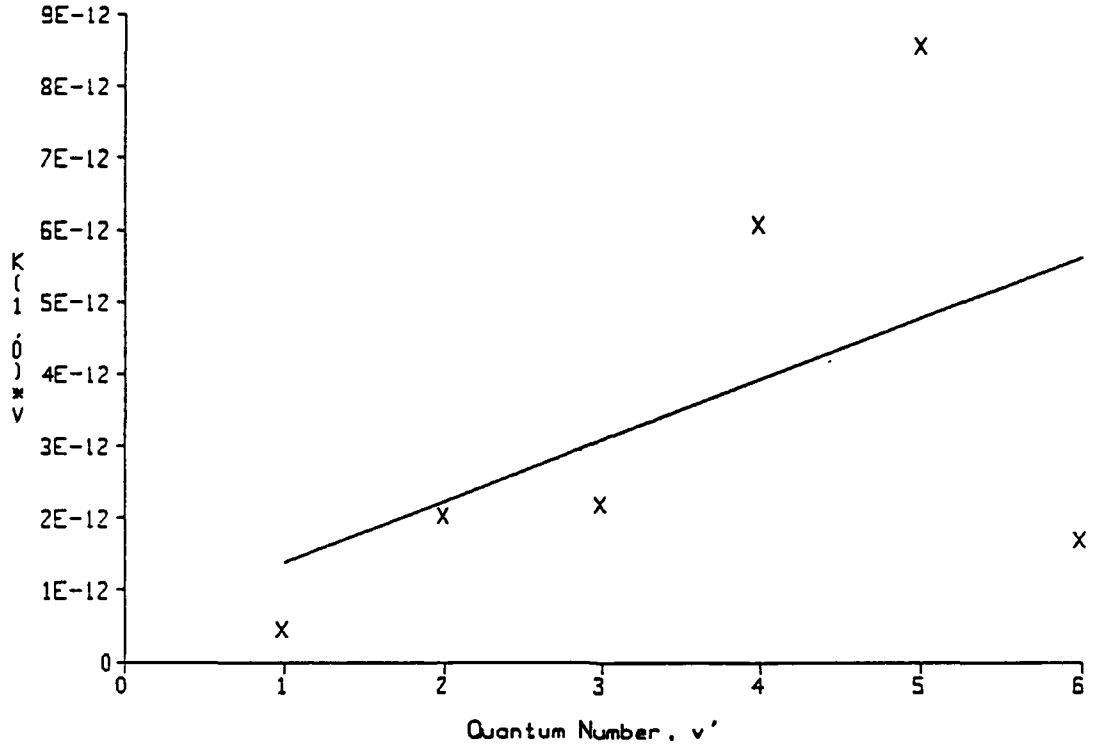

Figure 22. Landau-Teller fit to Argon data, v'= 1 - 6

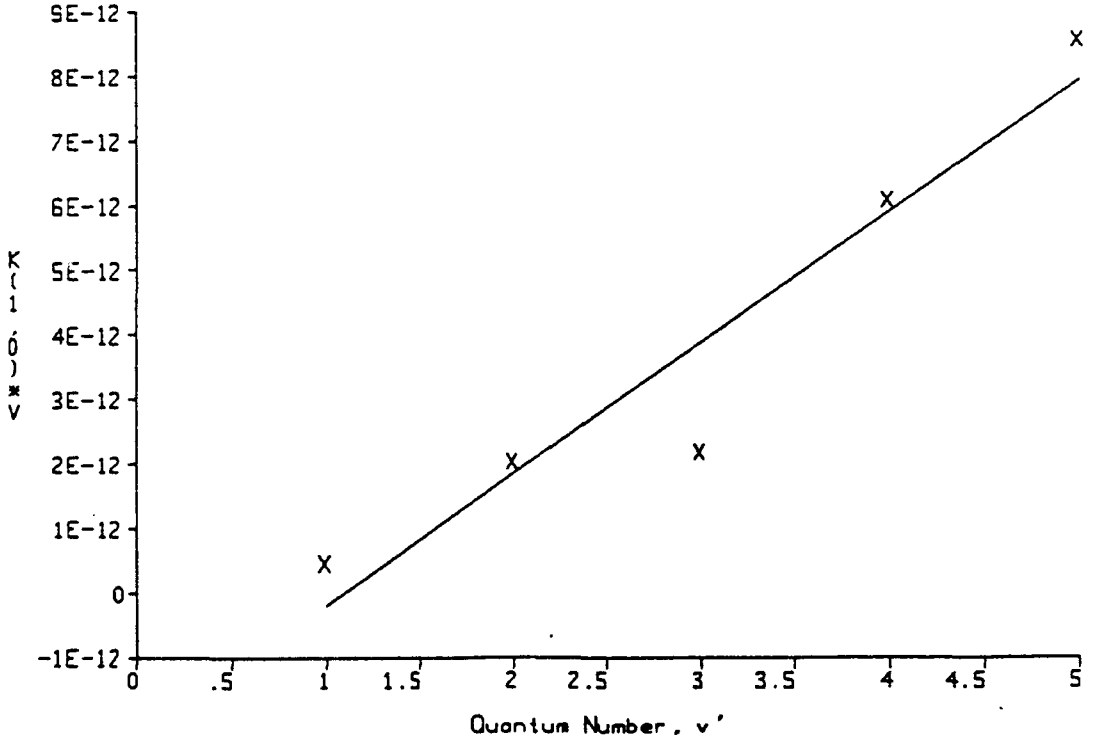

Figure 23. Landau-Teller fit to Argon data, v'= 1 - 5

Table VI. Fundamental Rate Coefficients with Argon Buffer Gas

v'	Rate Coefficient ($10^{-12}cm^3$/molecule·sec)
6	0.285 ± .05
5	1.716 ± .1
4	1.525 ± .05
3	0.641 ± .06
2	1.021 ± .05
1	0.463 ± .05
Avg $k_v(1,0)$ = 0.97 ± .5	

4.2.2 Helium. Helium was studied less in depth than argon after it was determined that argon obeys the Montroll-Shuler model and Landau-Teller scaling. Helium was studied by pumping v'= 5, observing transitions from v'= 4 and 2, and pumping v'= 2, observing transitions from v'= 1. As for the case of argon, the Montroll-Shuler fits were excellent for each transition, and the Stern-Volmer plots were linear. Also similar to argon, a transition observed with a high mix pressure (pump v'= 2, observe v'= 1) yielded a negative Stern-Volmer intercept and the lowest rate coefficient. Table VII gives the rate coefficients for the observed vibrational level and Figure 24 shows the Landau-Teller fit for

helium. Helium can be described by a fundamental rate coefficient $k_v(1,0) = (3.9 \pm .7)x10^{-12}$ $cm^3/(molecules \cdot sec)$.

Table VII. Fundamental Rate Coefficients with Helium Buffer Gas

v'	Rate Coefficient ($10^{-12}cm^3$/molecule·sec)
4	4.839 ± .15
2	3.916 ± .08
1	3 092 ± .15
Avg $k_v(1,0) = 3.9 \pm .7$	

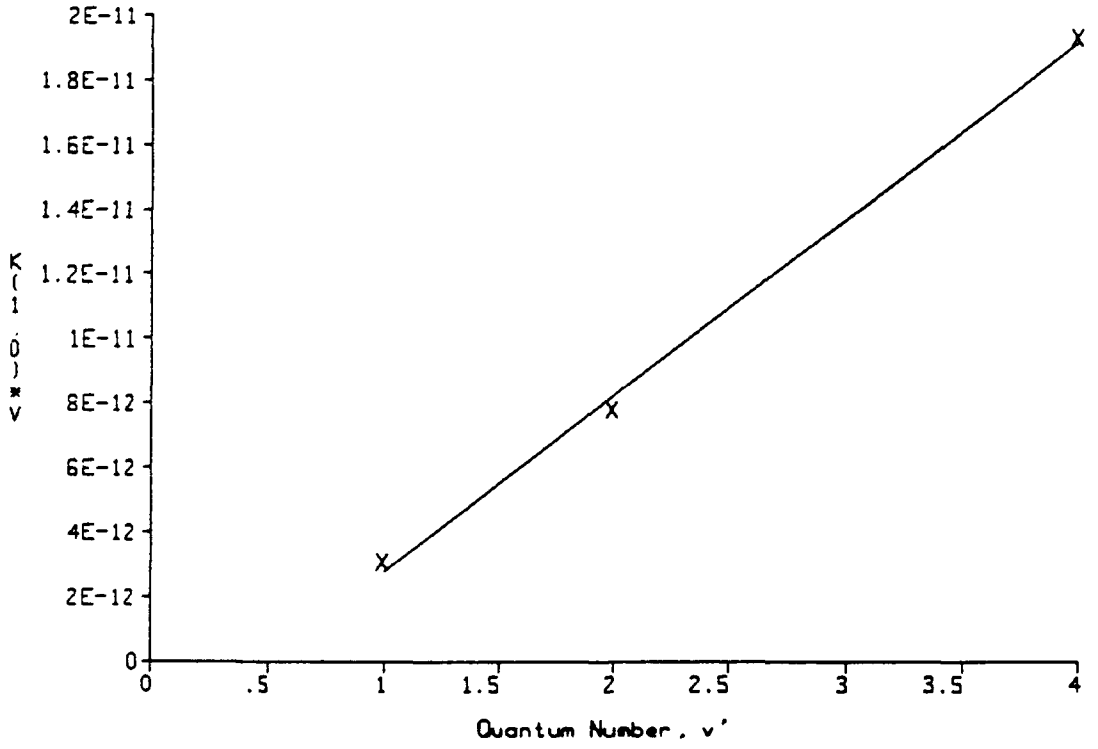

Figure 24. Landau-Teller fit to Helium data

4.2.3 Neon, Krypton and Xenon. After showing that argon and helium obey the Montroll-Shuler model and Landau-Teller scaling, the remaining rare gases were quickly studied. For neon, krypton and xenon, only the v'= 5 level was pumped and the transition from the v'= 4 level was observed. Again, the Montroll-Shuler fits were excellent and the Stern-Volmer fits were linear with good intercepts. All signals were strong so no transitions were studied with a high mix pressure. Table VIII provides the results.

Table VIII. Fundamental Rate Coefficients for Neon, Krypton and Xenon

Gas	Rate Coefficient ($10^{-12}cm^3$/molecule·sec)
Ne	1.02 ± .05
Kr	0.636 ± .02
Xe	0.224 ± .03

4.2.4 SSH Theory The Schwartz, Slawsky and Herzfeld theory predicts that the probability of vibrational transfer, $P = k_v/k_g$, is proportional to the (reduce mass)^{½} if the vibrational spacing is relatively large. For BrF, the gas kinetic cross-sections, reduced masses, relative velocities, and both the gas kinetic rate coefficients and the fundamental rate coefficients found for the experimental 5 → 4 data with each buffer gas are given in Table IX. The logarithm of the probability

is plotted versus the (reduced mass)$^{\frac{1}{2}}$ in Figure 25. As can be seen, there is considerable scatter in the rate coefficients, however the trend is correct and the slope is negative.

Table IX. Gas Kinetic Collision Parameters for BrF/Buffer Gas Collisions $k_v(5 \rightarrow 4)$[18,19]

Buffer Gas	Cross-section (Å^2)	Reduced Mass (a.u.)	Relative velocity (10^4 cm/s)	Gas Kinetic Rate Coeff. (10^{-10} cm^3/molec•sec)	Experimental Rate Coeff. (10^{-12} cm^3/molec•sec)	Prob-k_v/k_g
He	31.3	3.84	12.9	4.04	3.9	0.0096
Ne	33.5	16.6	6.2	2.08	1.02	0.0049
Ar	40.2	28.5	4.7	1.89	0.97	0.0051
Kr	42.4	45.4	3.7	1.57	0.636	0.0041
Xe	52.2	56.4	3.3	1.72	0.224	0.0013

4.2.5 Comparison to the Other Interhalogens Along with BrF (plotted as *) in Figure 25 are plotted points for I_2(x), BrCl(+) and IF(o).[3] As can be seen, IF obeys the SSH theory well, whereas I_2 and BrCl differ from SSH predictions substantially. BrF is in between IF and BrCl. Referring back to section 2.4.3, this is understandable: BrF is between IF and BrCl in terms of vibrational spacing and anharmonicity. IF obeys Montroll-Shuler and SSH because of its large vibrational spacing and low

anharmonicity. BrCl has a smaller vibrational spacing and worse anharmonicity so it is poorly modelled. From the relative magnitudes of probabilities it can be seen that IF and BrF, which have the largest vibrational spacings and lowest anharmonicities, are less likely to undergo vibrational energy transfer.

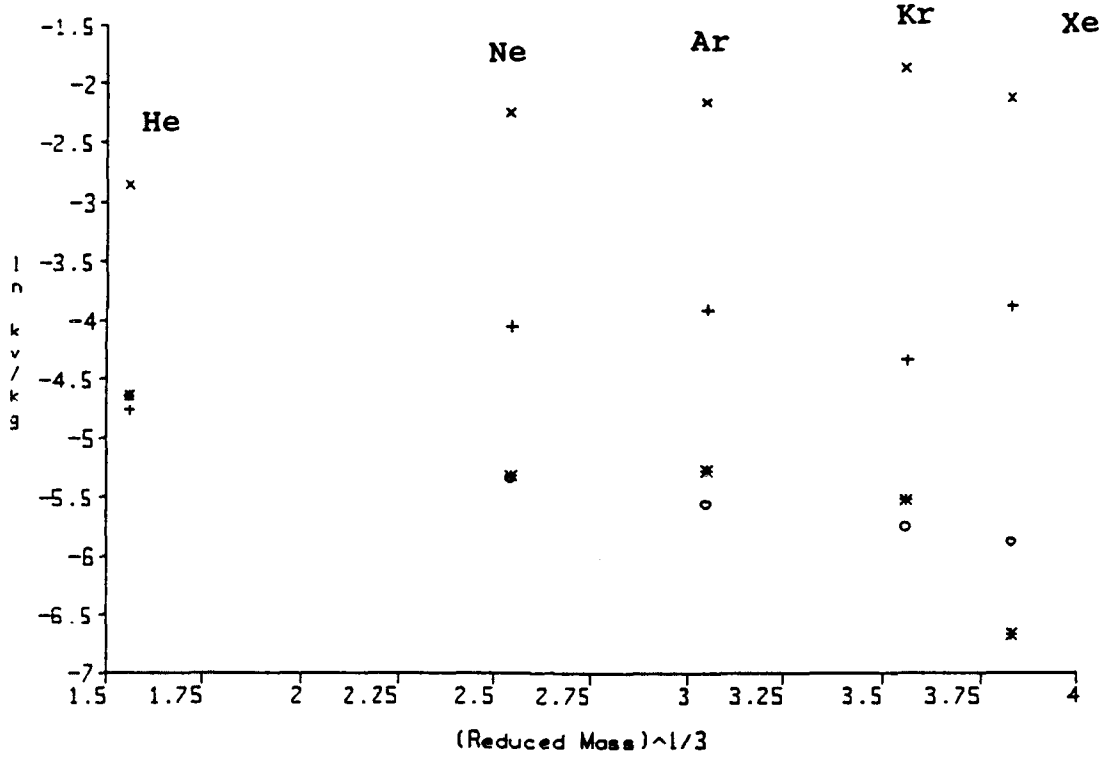

Figure 25. Demonstration of SSH theory

I_2 (x), BrCl (+), BrF (*), IF (o)

V. Conclusions and Recommendations

5.1 Conclusions

This study, in conjunction with the previous study by Melton, shows that, with some minor inconsistencies, vibrational energy transfer in BrF induced by the production mix can be well represented by the Montroll-Shuler model. Landau-Teller scaling is obeyed, and a single fundamental rate coefficient of $k_v(1,0) = (4.0 \pm 0.5) \times 10^{-12}$ $cm^3/(molecules \cdot sec)$ can be used to describe vibrational transfer rates at all vibrational levels below the predissociation level.

When vibrational transfer is induced by the rare gases, the Montroll-Shuler model and Landau-Teller scaling is again obeyed, within the limits of systematic errors. Fundamental rate coefficients range from a high for helium of $(3.9 \pm 0.7) \times 10^{-12}$ $cm^3/(molecules \cdot sec)$ to a low for xenon of $(2.2 \pm 0.3) \times 10^{-13}$ $cm^3/(molecules \cdot sec)$. Vibrational transfer induced by the rare gases was also found to obey the Schwartz, Slawsky and Herzfeld (SSH) theory which requires that the vibrational transfer probability $P_v(1,0)$ be proportional to the reduced mass of the collision partners.

5.2 Recommendations

The study performed here has been fairly complete for the collision pairs studied. The vibrational transfer induced by the

production mix has been examined across a broad range of both pump and transition vibrational levels. Additional study of self transfer would not be necessarily advantageous.

If signal strength can be increased by either increasing laser strength or detector efficiency, vibrational transfer induced by the rare gases should be briefly re-examined. The weaker transitions could not be studied without creating flow problems. These flow problems, which decreased the signal strength from run to run and affected the intercepts of the Stern-Volmer plots, also produced systematic errors in the rate coefficients. With a stronger signal, lower mix pressures can be used which should not disrupt the flow and should produce more accurate rate coefficients.

Another benefit in an increase in signal strength is it will allow the monochromator slits to be reduced. It will then be possible to focus the monochromator's resolution onto a single transition with less overlap from competing transitions. This will reduce the importance of overlap fractions and all the errors inherent in them.

An important area for further study would be to look at vibrational transfer induced by additional gases including O_2, N_2 and SF_6. SF_6 is especially interesting because of its low quenching rate and the possibly fast vibrational transfer rate suggested by Melton.[6] It would then be a feasible candidate as a bath gas to thermalize the BrF(B) without a high measure of electronic quenching.

Appendix A. BrF Spectroscopic Data

Figure 26 shows a portion of the vibrational spectrum of BrF from 5000Å to 6000Å. This was created by scanning the monochromator across the wavelength band of interest while pumping the v' = 6 vibrational level. Spectrums similar to this were used to select the best transitions to observe for vibrational transfer analysis. The following tables provide the most current spectroscopic data on BrF. Table X contains the latest estimates of collision free lifetimes for selected vibrational levels of BrF from Clyne.[20] Coxon[8] tabulates the vibrational constants and term values for ^{79}BrF and ^{81}BrF in Table XI. The Franck-Condon factors in Table XII were found from a computer code developed at the Phillips Lab using the latest RKR turning points found by Coxon.[6,8]

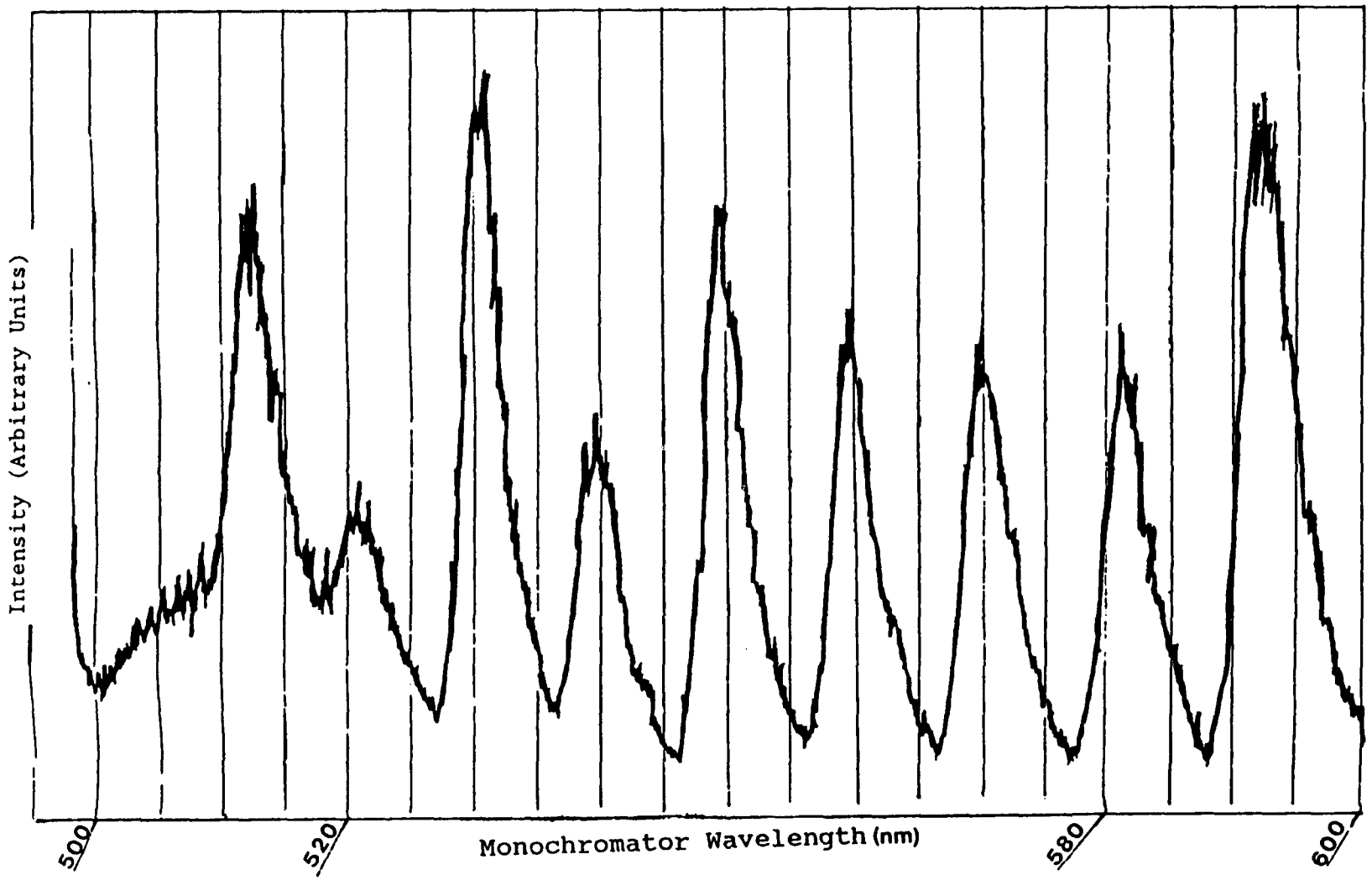

Figure 26. Partial BrF Vibrational Spectrum
Pressure = 760 mtorr, Slit Width = 1 mm

Table X. Collision-Free Lifetimes (μsec) for Selected Ro-vibrational Levels of BrF(B)[20]

v'	J'		^{79}BrF	^{81}BrF
7	28	predissociated	59.4	57.3
	27	predissociated?	60.1	60.1
	20	stable	65.2	65.5
	11	stable	63.2	62.8
6	48	predissociated	10.4	52.7
	47	predissociated	58.3	58.6
	46	predissociated	58.8	58.5
	45	stable	62.1	58.0
	21	stable	62.6	62.2
	10	stable	63.0	62.7
5	21	stable	58.9	—
4	21	stable	59.0	—
3	21	stable	55.5	—

Table XI. Spectroscopic Constants (cm^{-1})[8]

constant	^{79}BrF	^{81}BrF
T_8'	21038.809	21033.625
T_7'	20771.38	20766.342
T_6'	20482.367	20477.727
T_5'	20176.215	20172.067
T_4'	19855.327	19851.792
T_3'	19521.244	19518.385
T_2'	19175.037	19172.933
T_1'	18817.572	18816.324
T_0'	18449.496	18449.084
w_e''	669.823	668.227
$w_e''x_e''$	3.753	3.739
$w_e''y_e''$	-8.7×10^{-3}	-7.8×10^{-3}
$w_e''z_e''$	-1.6×10^{-4}	-2.0×10^{-4}

Table XII. Franck-Condon Factors for $^{79}BrF^{6}$

v' / v"	0	1	2	3	4
0	1.5445E-5	1.1966E-4	4.8959E-4	1.3974E-3	3.1188E-3
1	2.1606E-4	1.4001E-3	4.7702E-3	1.1283E-2	2.0759E-2
2	1.4464E-3	7.6189E-3	2.0862E-2	3.9106E-2	5.6029E-2
3	6.1916E-3	2.5539E-2	5.3406E-2	7.3812E-2	5.5207E-2
4	1.9043E-2	5.8433E-2	8.6108E-2	7.6353E-2	4.0487E-2
5	4.4641E-2	9.4618E-2	8.4906E-2	3.3285E-2	1.2660E-3
6	8.2835E-2	1.0795E-1	4.1805E-2	1.7712E-4	2.0442E-2
7	1.2516E-1	8.1424E-2	2.4322E-3	2.4885E-2	5.2424E-2
8	1.5671E-1	3.1506E-2	1.5062E-2	6.0264E-2	2.7870E-2
9	1.6449E-1	6.6587E-4	6.0865E-2	4.1162E-2	1.9670E-5
10	1.4411E-1	1.8042E-2	7.5189E-2	2.6541E-3	3.0173E-2
11	1.1048E-1	7.0836E-2	3.8212E-2	1.6740E-2	5.3237E-2
12	7.1595E-2	1.1890E-1	1.7748E-3	6.1311E-2	1.9527E-2
13	3.9961E-2	1.3231E-1	1.7122E-2	6.1071E-2	1.7076E-3
14	1.9217E-2	1.1071E-1	7.3143E-2	1.7305E-2	4.1296E-2
15	7.9625E-3	7.3679E-2	1.1943E-1	2.1556E-3	6.4795E-2

Table XII. Continued

v' / v"	5	6	7
0	5.7963E-3	9.3243E-3	1.3373E-2
1	3.1637E-2	4.1544E-2	4.8438E-2
2	6.5051E-2	6.3317E-2	5.2794E-2
3	5.5207E-2	2.9698E-2	9.7643E-3
4	9.1821E-3	9.6752E-5	8.8721E-3
5	8.8180E-3	2.9819E-3	3.7742E-2
6	4.4265E-2	3.5939E-2	1.2960E-2
7	2.8778E-2	2.1832E-3	5.0289E-3
8	1.2130E-6	1.7899E-2	3.3716E-2
9	2.7952E-2	3.8088E-2	1.3455E-2
10	4.2356E-2	7.0495E-3	4.2645E-3
11	7.2523E-3	1.0442E-2	3.3700E-2
12	1.0552E-2	4.0656E-2	1.5542E-2
13	4.7469E-2	1.6775E-2	3.0408E-3
14	3.1416E-2	2.8878E-3	3.4986E-2
15	9.9271E-5	3.9384E-2	2.2232E-2

Appendix B. Systematic Errors

No experimental apparatus is designed so well so as to avoid some systematic errors. Because the resolution of the monochromator covered more than the transition of interest, overlap fractions were required to compensate for overlapping transitions. Because of the necessity for a large variation in buffer gas pressure, BrF mix flow was disrupted during measurements. Also, no theory or model is so complete that it covers all variations. The Montroll-Shuler model assumes a number of restrictions that BrF doesn't necessarily follow. This appendix will briefly discuss these problems.

1. Overlap Fractions

Accounting for overlapping transitions with a single triangle function is at best a rough approximation for a procedure that should be done individually for each transition. The ideal solution is to account for the population in each vibrational level with a Maxwell-Boltzmann distribution. Then, overlapping Maxwell-Boltzmann distributions would determine which transitions were observed. Instead, a single triangle function was used with two parameters that can be adjusted to obtain the best fit to the data.

The size of the overlap fractions used were made by comparing the Montroll-Shuler fits with data. The data was first evaluated using the

same overlap fractions used by Melton. By adjusting the size of the overlap fraction while studying which transitions are involved, the Montroll-Shuler fits can be adjusted so as to optimize the quality of fit for all transitions. Overall, Melton's overlap fractions of 120Å and 34Å produced inconsistent fits and poor Stern-Volmer plots for this data. The rate coefficient from the self-transfer, pump 6, observe 4 data, using overlap fractions from Melton yielded a rate coefficient of $k_v(1,0) = 5.454 \times 10^{-12}$ cm^3/(molecules•sec). Comparing this with the rate coefficient of 3.864×10^{-12} cm^3/(molecules•sec) found from the data using overlaps of 100Å and 30Å, provides a rough estimate on the magnitude of error that the overlaps produce: 29%. The optimized overlap fractions of 100Å and 30Å were used throughout this study.

If a fit is noticeably skewed, then a possible reason is that other transitions are being observed in addition to the transition of interest. Optimizing the Montroll-Shuler fits by adjusting overlap fractions can improve the general quality of fits, but there will still be transitions with poor fits that can best be explained by incorrect overlap fractions. For example, the pump $v' = 6$, observe $v' = 0$ from the self-transfer data, shown in Figure 13, can be understood by postulating that the overlapping $v' = 7$ or $v' = 2$ transitions (see Table II) are more intense then the effective Frank-Condon factors would suggest. This would explain why the signal increases at a faster rate then the Montroll-Shuler model provides.

Once overlap fractions are chosen and in use, possible errors can also arise from uncertainties in the monochromator setting and in the

exact locations of the bandheads and widths of the overlapping transitions. This is especially true when the observation wavelength is slightly shorter than the bandhead wavelength. In this case the intensity of the overlap is changing very quickly with wavelength. If any wavelength calculation varies by a small amount than the intensity can change by a large amount and this will affect the Montroll-Shuler fit to the data.

For example, the pump v' = 6, observe v' = 6 (Figure 7) data has a strong overlapping v' = 2 transition which is on the long wavelength side of the observation wavelength. When this transition is accounted for in the Montroll-Shuler model, the fundamental rate coefficient from a Stern-Volmer plot is 2.74 $x10^{-12}$ $cm^3/(molecules \cdot sec)$. If this transition is neglected, which is equivalent to shifting the wavelength, either observation or bandhead, by only 5Å, then the rate coefficient is 4.18 $x10^{-12}$ $cm^3/(molecules \cdot sec)$. On some transitions overlap fractions are a substantial source of error.

2. Flow Disruptions

In the study involving vibrational transfer induced by buffer gases, the mix pressure was kept as low as possible while maintaining a strong signal. However, weak transitions required higher mix pressures which create a greater opportunity for the flow to be disrupted by the buffer gas. With high mix pressures, higher buffer gas pressures can substantially decrease the amount of mix that enters the chamber. There will then be more buffer gas and less mix gases in the chamber than is

assumed, and the rate coefficient output by the Montroll-Shuler model will attempt to compensate by being lower than it actually is.

Equation 17 demonstrates this. If the decay rate seen by the model is low, because of the low concentration of BrF and its relatively fast rate coefficient, then the model attempts to compensate by lowering the rate coefficient of the buffer gas. All other values are constants, input into the model.

$$\Gamma = 1/\tau_R + k_{BrF}[BrF] + k_{buffer}[buffer] \qquad (17)$$

In some cases the model compensates so much for the missing mix gas that it outputs a negative rate coefficient. These rate coefficients were then plotted with the standard Stern-Volmer technique to produce the rate coefficients reported, but the intercepts of the Stern-Volmer plots are strongly negative.

Using typical values for the buffer gas pressure, k_{buffer} and k_{BrF}, the effect of fluctuations in the mix pressure is negligible for pressures of about 100 mtorr or less. The strongest signals required mix pressures of about 100 mtorr. The weaker signals, which had the negative intercepts and large error bounds on the rate coefficients, required mix pressures up to 200 mtorr.

Two methods were used to reduce the data for the transfer induced by buffer gases. For the first method, the coefficient for self-transfer, k_{BrF}, found earlier, was input into the model. The output of the model was then the buffer gas rate coefficient, k_{buffer}. The second

method fit the data to a single rate coefficient, and then use a Stern-Volmer technique with the partial pressures of the buffer gases to obtain the buffer gas rate coefficient. Both methods produced identical rate coefficients for the buffer gas. Also, the second method provided an additional check on the self-transfer rate coefficient, because the product of it and the mix concentration is the intercept in the Stern-Volmer plot.

The argon pump 6, observe 3 data was produced with a mix pressure of 150 mtorr. Reducing this data using the second method yielded a self-transfer rate coefficient of 3.65 $x10^{-12}$ $cm^3/(molecules \cdot sec)$ from the intercept of the Stern-Volmer plot. With this intercept and the 4.0 $x10^{-12}$ $cm^3/(molecules \cdot sec)$ average value found for self-transfer gives a mix pressure of 136.7 mtorr. This is an error of 9%. There was 9% less BrF mix in the chamber then originally measured due to disruption in the flow by the buffer gas. This provides a rough approximation of the error associated with the disruption of the flow, however this error is a function of mix pressure.

3. *Model Deficiencies*

Figures 7 - 13 show that the Montroll-Shuler model fits fairly well with these transitions. The transitions with the poorest fits are from $v' = 2$, 1, and 0, shown in Figures 11 - 13. Multi-quantum transfer is a possible explanation for these poor fits, in that the Montroll-Shuler model assumes vibrational transfer of $\Delta v' = \pm 1$ only. Multi-quantum transfer would reveal itself by a slow trend with decreasing v'

of a stronger intensity earlier than predicted by the Montroll-Shuler model. This is not always the case as can be seen in the Figures. Figures 11 and 13 do show an early strong intensity, but these can also be explained by a poor choice of overlap transitions. Multi-quantum transitions are certainly a possible phenomenon in BrF, but only seem to affect data gathered from low level transitions, which are widely separated from the pump level.

Predissociation is another characteristic which can affect the data. The Montroll-Shuler model does not consider predissociation, and at low vibrational level it should not be a problem. However for the pump v'= 6 data, approximately half of the population that transfers up into the v'= 7 level will be lost. This may be revealed in the large intercepts on the Stern-Volmer plots. The rate coefficient will be artificially high if a substantial portion of the population is lost to predissociation. At lower pressures, where less of the population can transition upward, the rate coefficient will be lower. However, the Stern-Volmer plot does not show any curvature (Figure 14). This may mean that the vibrational level spacing in BrF, $\Delta E_v = h\nu/k_BT = 1.7$, is large enough to prevent much of the population from transitioning upward into a higher J' level of v' = 7.

Another possible characteristic which is not accounted for by the Montroll-Shuler model is any dependence of the radiative lifetime, τ_R, on the vibrational level. If τ_R is a function of v', than its affect on the rate coefficient would depend on that functionality. If τ_R decreases with increasing v', than the rate coefficients will increase.

Any effect would be exhibited in a Landau-Teller plot (Figure 15) which is fairly linear. From the quality of the data, any dependence that τ_R may have must be very weak, because there is not a strong trend seen that can be traced to radiative lifetime being a function of v'.

Bibliography

1. Perram, G.P., "Visible Chemical Lasers", *Proceedings of the International Conference on Lasers, 1989*, STS Press (1990).

2. Davis, S.J., "Prospects for Visible Chemical Lasers", SPIE Vol 540, Southwest Conference on Optics (1985), P188.

3. Perram, G.P., "Collisional Dynamics of the $B^3\pi(0+)$ State of Bromine Monochloride," Dissertation, AFIT DS-86, (1986).

4. Wolf, P.J., "Collisional Dynamics of the $B^3\pi(0+)$ State of Iodine Monofluoride," Dissertation, AFIT DS-85, (1985).

5. Lowe, B.F., "Energy Transfer in Singlet Oxygen and Bromine Monofluoride," Master's Thesis, AFIT GEP-90D, (1990).

6. Melton, D.W., "Collisional Dynamics of the $B^3\pi(0+)$ State of Bromine Monofluoride," Dissertation, AFIT DS-91, (1991).

7. Clyne, M.A.A and I.S. McDermid, "Quantum Resolved Dynamics of Excited States – Part 2: Stable Levels of the $B^3\pi(0^+)$ State of BrF," *Journal of the Chemical Society, Faraday Transactions II.*, 74: 664 (1978b).

8. Coxon, J.A. and M.A. Wickramaaratchi, "The $B^3\pi(0+) \rightarrow X^1\Sigma^+$ Emission Spectrum of ^{79}BrF and ^{81}BrF in the Range 6250-8700A," *Journal Molecular Spectroscopy*. 87: 85 (1981).

9. Steinfeld, J.I. *Molecules and Radiation*. Cambridge: MIT Press, 1985.

10. Clyne, M.A.A. and I.S. McDermid, "Laser-induced Fluorescence: Electronically Excited States of Small Molecules", *Dynamics of the Excited State*, Edited by K.P. Lowley. J.Wiley and Sons (1982).

11. Perram, G.P., Class Notes, Chem 720, Kinetics of Fast Reactions. AFIT/ENP, May 1991.

12. Landau, V.L. and E. Teller, *Phys Z Sowj Un*. 10: 35 (1936).

13. Montroll, E.W. and K.E. Shuler, "Studies in Nonequilibrium Rate Processes. I. The Relaxation of a System of Harmonic Oscillators," *Journal Chemical Physics*. 26: 454 (1957).

14. The code for this application of the Montroll-Shuler model was written and tested by D.W. Melton. See reference 6, Appendix B.

15. Schwartz, R.M., Z.I. Slawsky and K.F. Herzfeld, *Journal of Chemical Physics*, 20, 1591, (1952).

16. Bemand, P.P., and M.A. Clyne, "Kinetic Spectroscopy in the Far Ultraviolet." *Journal of the Chemical Society, Faraday Transactions II*, 72: 191 (1976).

17. Clyne, M.A.A., A. Curran and J.A. Coxon. "Studies of Labile Molecules with a Tunable Dye Laser - Laser Excitation Spectrum of BrF ($B^3\pi(0^+) - X^1\Sigma$)." *Journal of Molecular Spectroscopy*. 63: 43 (1976).

18. Hirschfelder, J.O., C.F. Curtiss and R.B. Bird, *Molecular Theory of Gases and Liquids*. John Wiley and Sons, Inc. (1954).

19. Fischer C. F., *Atomic Data*, 4, 305-316, (1972).

20. Clyne, M.A.A. and J.P. Liddy, "Quantum-resolved Dynamics of Excited States. Part 6.-Radiative Lifetime and Collisional Deactivation Rates in BrF(B)." *Journal of the Chemical Society, Faraday Transactions II*, 76, 1569, (1980).